LIMNOLOGY and OCEANOGRAPHY

ASLO

Limnol. Oceanogr. 61, 2016, 1301–1321

doi: 10.1002/lno.10291

Particulate matter stoichiometry driven by microplankton community structure in summer in the Indian sector of the Southern Ocean

M. Rembauville,*[1] S. Blain,[1] J. Caparros,[1] I. Salter[1,2]

[1]Sorbonne Universités, UPMC Univ Paris 06, CNRS, Laboratoire d'Océanographie Microbienne (LOMIC), Observatoire Océanologique, Banyuls/mer, France

[2]Alfred Wegener Institute, Helmholtz Centre for Polar and Marine Research, Bremerhaven, Germany

Abstract

Microplankton community structure and particulate matter stoichiometry were investigated in a late summer survey across the Subantarctic and Polar Front in the Indian sector of the Southern Ocean. Microplankton community structure exerted a first order control on PON:POP stoichiometry with diatom-dominated samples exhibiting much lower ratios (4–6) than dinoflagellate and ciliate-dominated samples (10–21). A significant fraction of the total chlorophyll *a* (30–70%) was located beneath the euphotic zone and mixed layer and sub-surface chlorophyll features were associated to transition layers. Although microplankton community structure and biomass was similar between mixed and transition layers, the latter was characterized by elevated Chl:POC ratios indicating photoacclimation of mixed layer communities. Empty diatom frustules, in particular of *Fragilariopsis kerguelensis* and *Pseudo-nitzschia*, were found to accumulate in the Antarctic Zone transition layer and were associated to elevated BSi:POC ratios. Furthermore, high $Si(OH)_4$ diffusive fluxes (>1 mmol m^2 d^{-1}) into the transition layer appeared likely to sustain silicification. We suggest transition layers as key areas of C and Si decoupling through (1) physiological constraints on carbon and silicon fixation (2) as active foraging sites for grazers that preferentially remineralize carbon. On the Kerguelen Plateau, the dominant contribution of *Chaetoceros Hyalochaete* resting spores to microplankton biomass resulted in a three-fold enhancement of POC concentration at 250 m, compared to other stations. These findings further highlight the importance of diatom resting spores as a significant vector of carbon export through the intense remineralization horizons characteristing Southern Ocean ecosystems.

The Southern Ocean connects the three major Ocean basins and is important for heat and carbon exchange with the atmosphere, representing a critical conduit by which anthropogenic CO_2 enters the ocean (Sabine et al. 2004; Khatiwala et al. 2009). Modeling studies have suggested that nutrients exiting the Southern Ocean, through the formation of mode water, may constrain primary production in vast areas of the global Ocean (Sarmiento et al. 2004; Dutkiewicz et al. 2005). The efficiency and stoichiometry of surface nutrient depletion by the biological pump in the Southern Ocean can thus have major implications for global Ocean productivity (Primeau et al. 2013). A large fraction of present-day Southern Ocean surface waters are referred to as "High-Nutrient, Low-Chlorophyll" areas (HNLC, Minas et al. 1986) where low trace-metal concentrations, in particular iron, can limit primary production (de Baar et al. 1990; Martin 1990) and result in a weaker biological pump (e.g., Salter et al. 2012). Regional trace metal inputs from shelf sediments and glacial melt-water can sustain large scale (>100 km) and long lasting (several months) phytoplankton blooms in proximity to island systems such as South Georgia, Crozet and Kerguelen plateaus (Whitehouse et al. 2000; Blain et al. 2001; Pollard et al. 2007).

Many studies of phytoplankton blooms in the Southern Ocean usually focus on the euphotic zone and studies using satellite data (e.g., Park et al. 2010; Borrione and Schlitzer 2013) are restricted to the surface. However, subsurface chlorophyll maxima (SCM) deeper than the euphotic zone at the base of the mixed layer are recurrent in late summer in the HNLC waters of the Southern Ocean (Parslow et al. 2001, Holm-Hansen and Hewes 2004; Holm-Hansen et al. 2005). Sub-surface chlorophyll features were also observed over the productive central Kerguelen Plateau in late summer (February) with chlorophyll *a* concentrations > 2.5 μg L^{-1} (Uitz et al. 2009), suggesting that SCM are not strictly

*Correspondence: rembauville@obs-banyuls.fr

Additional Supporting Information may be found in the online version of this article.

restricted to the HNLC waters. These sub-surface biomass features are observed around 100 m and thus escape satellite detection depth (~20 m in productive areas; Gordon and McCluney 1975). This region of the water column, also called the "transition layer," is defined as the interface between the stratified ocean interior and the highly turbulent surface mixed layer (Johnston and Rudnick 2009).

Diatoms typically dominate spring/summer phytoplankton blooms in the Southern Ocean (Korb and Whitehouse 2004; Armand et al. 2008; Quéguiner 2013), and the subsurface chlorophyll maximum is also characterized by a dominance of diatom biomass (Kopczynska et al. 2001; Armand et al. 2008; Gomi et al. 2010). Both studies from Armand et al. (2008) and Gomi et al. (2010) described a similarity between the mixed layer and deep diatom communities. However, Kopczynska et al. (2001) reported a difference between the mixed layer and the subsurface phytoplankton diatom assemblage with a dominance of larger species in the deeper samples. Additionally, high regional and interannual variability of diatom assemblages in the SCM is reported from two consecutive summer surveys in the Polar Frontal Zone (PFZ) and the Seasonal Ice Zone in the Indian Sector of the Southern Ocean (Gomi et al. 2010).

It has been proposed that the development of sub-surface biomass features in the Southern Ocean is linked to iron depletion in the mixed layer (Parslow et al. 2001). Under these conditions, phytoplankton accumulates in temperature minimum layers that are frequently associated to the pycnocline and/or nutricline (Holm-Hansen and Hewes 2004). The similarity that is frequently observed between mixed layer and the SCM diatom communities supports this hypothesis (Armand et al. 2008; Gomi et al. 2010). It is presently unclear, however, if the SCM phytoplankton communities are predominantly senescent and/or poorly active (Parslow et al. 2001; Armand et al. 2008) or productive communities with low growth rates sustained by nutrient diffusion through the pycnocline (Holm-Hansen and Hewes 2004; Quéguiner 2013). Irrespective of photosynthetic production levels, it has been suggested previously that the transition layer could be an important foraging site for various micro- and mesozooplanktonic grazers (Kopczynska et al. 2001; Gomi et al. 2010). A coupled study of microplankton assemblages and particulate matter stoichiometry is therefore of particular importance to gain a better understanding of SCM formation and their impact on carbon and biomineral cycling through transition layers in the Southern Ocean.

Redfield (1958) first described the homogeneity of deep water N and P stoichiometry and its coherence with plankton stoichiometry and the resulting "Redfield-ratio" has been a central tenet in modern oceanography. The quantity of particulate matter data has increased substantially in recent years and stoichiometric nutrient ratios are commonly observed to derivate from Redfield values. A recent large scale data synthesis demonstrated that PON:POP ratios are not homogeneous at a global scale and may reflect latitudinal patterns related to plankton community composition (Martiny et al. 2013). Diatoms, for example, are known to have a lower N:P ratio than dinoflagellates or chlorophyceae (Ho et al. 2003; Quigg et al. 2003; Sarthou et al. 2005).

There are alternative explanations for latitudinal trends in particulate matter stoichiometry. The growth rate hypothesis (Elser et al. 1996) suggests that among one phytoplankton taxa, changes in physiological status affects the allocation of nutrients to various macromolecular pools with different N:P stoichiometry. For example, competitive equilibrium in nutrient limiting conditions will lead to the synthesis of N-rich proteins required for nutrient acquisition. During exponential growth, there is an increased demand for the synthesis of P-rich ribosomes which are required for cell component synthesis. (Elser et al. 1996; Sterner and Elser 2002; Klausmeier et al. 2004). This general scheme might be modulated by local availability of nutrients, and phytoplankton for example have been reported to synthesize nonphosphorous lipids in oligotrophic, low P environments (Van Mooy et al. 2009). Temperature has also been identified as a factor strongly influencing the N:P ratios and Southern Ocean diatoms contain more P-rich rRNA at low temperatures (Toseland et al. 2013). These observations reinforce the need of a joint description of plankton community structure and stoichiometry to document how plankton biogeography might impact Southern Ocean nutrient stoichiometry at local scale (Weber and Deutsch 2010).

In this study, we report data acquired late summer in the Subantarctic Zone (SAZ), the PFZ, and the Antarctic Zone (AAZ) in the Indian Sector of the Southern Ocean. Our objectives are (1) to assess whether patterns in sub-surface chlorophyll features are linked to biomass accumulation at physical interfaces, (2) to compare microplankton assemblages between the mixed layer and transition layer and identify physiological changes and potential ecological processes occurring within the transition layer, (3) investigate the statistical relationship between microplankton community structure and particulate matter stoichiometry in contrasting hydrological environments, and (4) to assess how biogeochemical processes within the transition layer modulate the intensity and stoichiometry of the particulate matter transfer from the mixed layer to the mesopelagic ocean.

Material and procedures

OISO23 cruise and sampling strategy

The OISO23 cruise took place onboard the R/V *Marion Dufresne* in the Indian sector of the Southern Ocean from the 06 January 2014 to the 23 February 2014. The biogeochemical study presented here is focused on 11 stations located on a latitudinal transect in the SAZ, PFZ, and AAZ, linking the two island systems of Crozet and Kerguelen (Fig. 1; Table 1). Conductivity-Temperature-Depth (CTD,

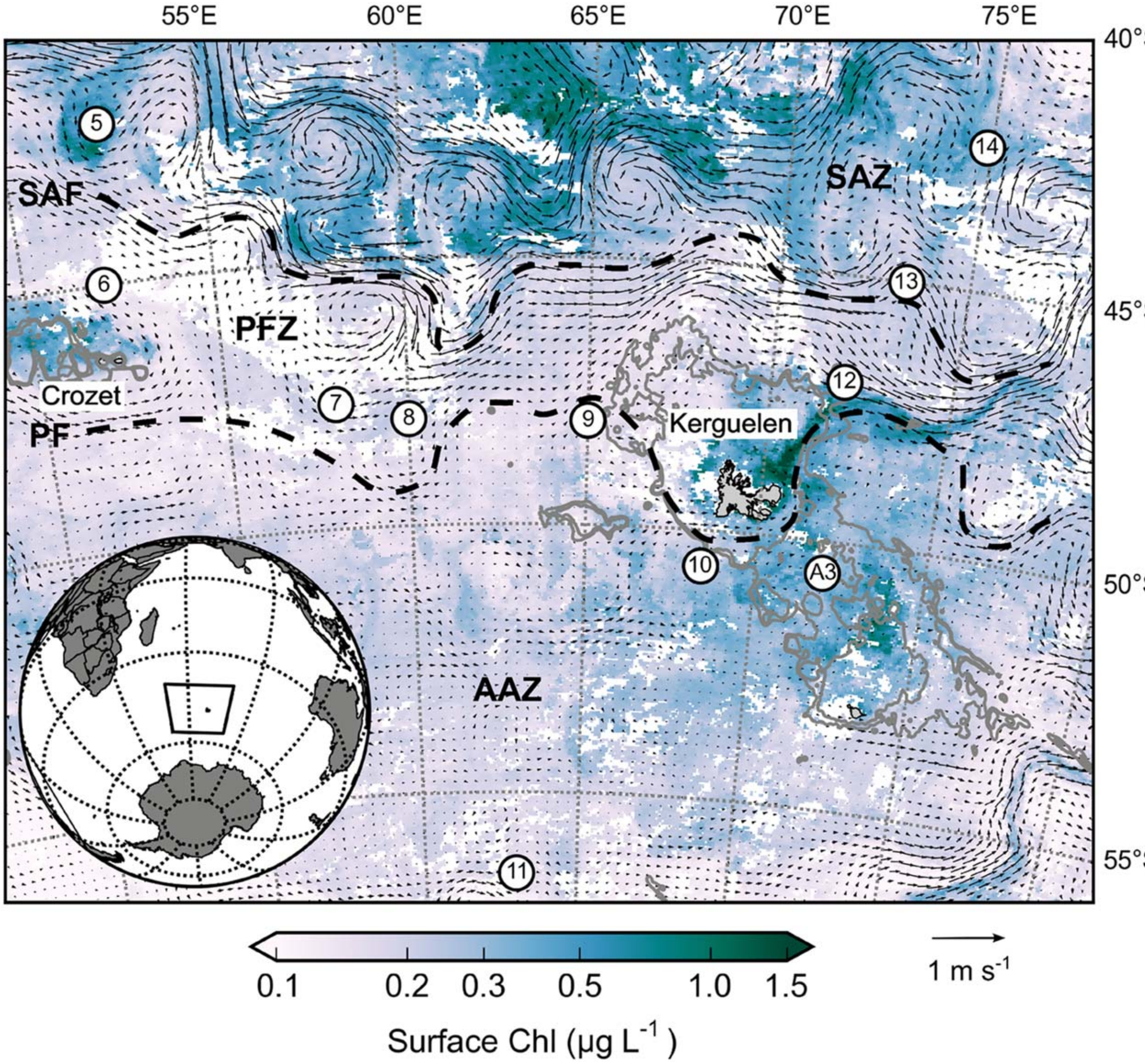

Fig. 1. Location of the study in the Indian sector of the Southern Ocean and station map. Satellite-derived surface chlorophyll *a* (MODIS level 3 product, 8 d composite) was averaged from 09 January 2013 to 10 February 2014. Arrows correspond to altimetry-derived geostrophic velocities (AVISO MA-DT daily product) averaged over the same period. Grey lines represent the 500 m and 1000 m isobaths. SAF, Subantarctic Front; PF, Polar Front; SAZ, Subantarctic Zone; PFZ, Polar Frontal Zone; AAZ, Antarctic Zone. [Color figure can be viewed in the online issue, which is available at wileyonlinelibrary.com.]

Seabird SBE 911 plus) casts were performed at each station. Samples for nutrients and chlorophyll *a* (Chl *a*) analyses were taken at 20 fixed depths. Precise sampling depths for particulate matter and microplankton abundance were chosen at each station following a preliminary analysis of the down-cast temperature, salinity, and fluorescence profiles. Samples were taken in the mixed layer, in the strong density gradient beneath the mixed layer (transition layer) and at a constant depth of 250 m. The last depth was chosen as a reference depth located under the annual upper mixed layer for this sector of the Southern Ocean (Park et al. 1998; de Boyer Montégut et al. 2004).

Derived hydrological parameters

The turbulent diffusivity coefficient was computed with the Thorpe scale method using the Shih et al. (2005) parameterization as previously described in Park et al. (2014). The robustness of the Thorpe scale calculation using this indirect method depends on the level of CTD processing prior to the computation (Park et al. 2014). The diffusivity coefficient (Kz in $m^2\ s^{-1}$) was calculated as follows:

$$\mathrm{Kz} = 1.6\ \nu^{1/2}\quad L_t\ N^{1/2} \tag{1}$$

where ν is the cinematic viscosity of seawater (1.5–1.8 10^{-6} $m^2\ s^{-1}$ for $T = 0$–5°C), L_t is the Thorpe scale (vertical density

Table 1. Stations labels, date and locations and attributed hydrological zone. Mixed layer depth (MLD), depth of the euphotic layer (Ze), depth of the fluorescence-derived chlorophyll maximum (Chl_{max}), and percentage of chlorophyll *a* located under the mixed layer depth.

Station	Date	Location	Zone	MLD (m)	Ze (m)	Depth of Chl_{max} (m)	% Chl under MLD
5	11 Jan 14	42°30′S 52°29′E	SAZ	35	35	20	39
6	12 Jan 14	44°60′S 52°06′E	PFZ	52	53	75	73
7	14 Jan 14	47°40′S 58°00′E	PFZ	59	58	46	54
8	16 Jan 14	48°00′S 60°00′E	PFZ	63	44	44	46
9	17 Jan 14	48°30′S 65°01′E	AAZ	70	42	77	58
10	19 Jan 14	50°40′S 68°25′E	AAZ	76	38	48	28
11	21 Jan 14	56°30′S 62°59′E	AAZ	71	66	61	65
A3	23 Jan 14	50°38′S 72°05′E	AAZ	78	37	50	53
12	06 Feb 14	46°60′S 72.01°E	PFZ	56	58	70	69
13	06 Feb 14	44.60°S 73.20°E	SAZ	39	44	47	50
14	08 Feb 14	42.28°S 74.54°E	SAZ	38	49	50	70

overturning scale, in m) and N is the Brunt-Väisalä buoyancy frequency (s^{-1}) defined as:

$$N = \left(-\frac{g}{\rho_e} \times \frac{d\rho}{dz}\right)^{1/2} \qquad (2)$$

where g is the gravitational acceleration (9.81 m s^{-1}), ρ_e is a constant reference density for seawater, ρ is the seawater density and z is the depth (m). Brunt-Väisälä buoyancy frequency was used to quantify the water column stability and the strength of the physical interface associated with the transition layer. Each Kz profile was averaged in 10 m bins. The Thorpe scale method cannot resolve overturns smaller than 20 cm, consequently Kz values $< 10^{-5}$ m^2 s^{-1} were set to this minimal value based on in situ measurements around the Kerguelen plateau with a Turbo MAP profiler (Park et al. 2014).

The mixed layer depth (MLD) was calculated using a 0.02 kg m^{-3} density-difference criterion relative to the density at 20 m (Park et al. 1998). The depth of the euphotic layer (Ze, 1% of the surface irradiance, in m) was calculated from the vertical profile of fluorescence-derived Chl *a* using Morel and Berthon (1989) formulation:

$$\mathrm{Ze} = 568.2 \left(\int_0^z \mathrm{chla}\ dz\right)^{-0.746} \qquad (3)$$

where chla is the Chl *a* concentration (mg m^{-3}) derived from the calibrated CTD fluorometer (WET Labs ECO FL, see below for calibration method). The calculation was performed iteratively downward from the surface until $z = \mathrm{Ze}$.

Biogeochemical analyses

Particulate matter: particulate organic carbon (POC), nitrogen (PON), phosphorous (POP), biogenic silica (BSi) and Chl a analysis

For POC and PON, 2 L of seawater were filtered on precalcinated (450°C, 24 h) 25 mm Whatman GF/F filters stored in precalcinated glass vials and dried overnight at 60°C. Filters were decarbonated by fumigating pure HCl (Merck) during 10 h. POC and PON were measured on a Perkin Elmer C,H,N 2400 autoanalyser calibrated with acetanelyde. Detection limits were defined as the mean blank plus three times the standard deviation of the blanks and were 0.17 μmol L^{-1} and 0.04 μmol L^{-1} for POC and PON, respectively. For POP, 500 mL of seawater was filtered on precalcinated GF/F filters. POP was analyzed following a wet oxidation procedure (Pujo-Pay and Raimbault 1994). Extracts were filtered through two precalcinated GF/F filters prior to spectrophotometric analysis of PO_4^{3-} on a Skalar autoanalyser following the method of Aminot and Kerouel (2007). The detection limit for POP was 0.01 μmol L^{-1}.

For BSi, 1 L of seawater was filtered on 25 mm nuclepore filter of 0.2 μm porosity. Filters were placed in cryotubes and dried at 60°C overnight. BSi was estimated by the triple NaOH/HF extraction procedure allowing correction of lithogenic silica (LSi, Ragueneau et al. 2005). Filters were digested two times with 0.2 N NaOH at 95°C during 45 min. At the end of both extractions, aliquots were taken for silicic acid ($Si(OH)_4$) and aluminum (Al) concentration measurements. A third extraction was performed with 2.9 N HF over 48 h at ambient temperature (~20°C). $Si(OH)_4$ was determined colorimetrically on a Skalar autoanalyser following Aminot and Kerouel (2007) and Al was determined fluorimetrically using the Lumogallion complex (Howard et al. 1986). The detection limit for BSi was 0.02 μmol L^{-1}. The LSi correction was most important in the vicinity of the plateaus (e.g., at A3, 250 m the LSi represented 17% of the total particulate Si).

For Chl *a* analysis, 2 L of seawater were collected in opaque bottles, filtered onto GF/F filters and immediately placed in cryotubes at −80°C. Pigments were extracted in 90% acetone solution and analyzed using 24 fluorescence excitation and emission wavelengths with a Hitachi F-4500 fluorescence spectrophotometer according to Neveux and Lantoine (1993). These Chl *a* concentrations measured from niskin bottles were used to calibrate the CTD fluorescence profiles by linear regression ($R^2 = 0.8$).

Dissolved nutrients analysis and calculation of diffusive fluxes

For the analysis of major nutrients (NO_3^-, NO_2^-, $Si(OH)_4$, PO_4^{3-}), 20 mL of filtered (0.2 μm cellulose acetate filters) seawater was sampled into scintillation vials and poisoned with 100 μL of 100 mg L^{-1} $HgCl_2$. Nutrient concentrations were determined colorimetrically on a Skalar autoanalyzer following Aminot and Kerouel (2007). Nutrient gradients were calculated at each sampling depth for particulate matter and microplankton based on the three nutrient concentrations (C) windowing this depth. Nutrient diffusive fluxes (N_{diff} in μmol m^{-2} s^{-1}) in the transition layer were calculated as follow:

$$N_{\mathrm{diff}} = Kz\frac{dC}{dz} \tag{4}$$

Kz profiles are highly variable over short time scales (days to hour), whereas nutrient gradients result from nutrient consumption occurring at longer timescales (weeks to month). To minimize the bias caused by short term Kz variability, nutrient diffusive fluxes were calculated using the average Kz profile from the study region (Supporting Information Fig. S1). A characteristic value of 4.5×10^{-5} m^2 s^{-1} in the transition layer was derived from the mean Kz profile.

Microplankton abundance, identification and biomass calculation

Seawater samples for microplankton identification and enumeration were collected in 125 mL amber glass bottles and immediately fixed with acid Lugol solution (1% final concentration). Samples were maintained in the dark at ambient temperature until counting (performed within 3 months after the sampling). Microplankton cells were enumerated from either a 50 mL (mixed layer and transition layer) or 100 mL (250 m) subsample after settling for 24 h (dark) in an Utermöhl counting chamber. Taxonomic identification was performed under an inverted microscope (Olympus IX71) with phase contrast at ×200 and ×400 magnification. One half of the counting chamber (mixed layer and transition layer) or the entire surface (250 m samples) was used to enumerate the microplankton. The total number of cells counted was > 200 except in sample 13 at 250 m. Ciliates and tintinnids were enumerated but not classified into taxa. Dinoflagellates were identified to the genus level, and diatoms were identified to species level when possible, following the recommendations of Hasle and Syvertsen (1997). Full and empty diatoms frustules were enumerated separately. Half or broken frustules were not considered. Due to the preserved cell contents sometimes obscuring taxonomic features on the valve face, taxonomic identification of diatoms to the species level was occasionally difficult and necessitated the categorizing of diatom species to genus or taxa as previously described in Rembauville et al. (2015a). The microplankton cell counts and empty diatom cell counts are provided in Supporting Information Tables S2 and S3, respectively.

The composition of living diatom biomass was estimated from the abundance of full cells using a species-specific carbon content for diatoms in the Indian sector of the Southern Ocean (Cornet-Barthaux et al. 2007). For species absent from this reference, > 20 individuals were measured from microscopic images using the imageJ software. Cell volume for the appropriate shape was calculated following Hillebrand et al. (1999) and carbon content was calculated using a diatom-specific carbon:volume relationship (Menden-Deuer and Lessard 2000). The same procedure was used for dinoflagellates and ciliates. For *Chaetoceros Hyalochaete* resting spores (CRS), the carbon content for spores over the Kerguelen plateau calculated in Rembauville et al. (2015a) was used. A complete list of microplankton categories and their respective carbon content is provided in Supporting Information Table S1.

Statistical analyses

To compare microplankton community structure between samples, Bray-Curtis distance was calculated based on raw microplankton abundances. Samples were clustered using the unweighted pair group method with arithmetic mean (UPGMA). To link microplankton community structure with biogeochemical factors (particulate matter stoichiometry and nutrient diffusive fluxes), a canonical correspondence analysis (CCA) was performed (Legendre and Legendre 1998). Prior to the CCA, microplankton abundances were sorted into groups to facilitate the ecological interpretation of the analysis. For example, a distinction is often made between

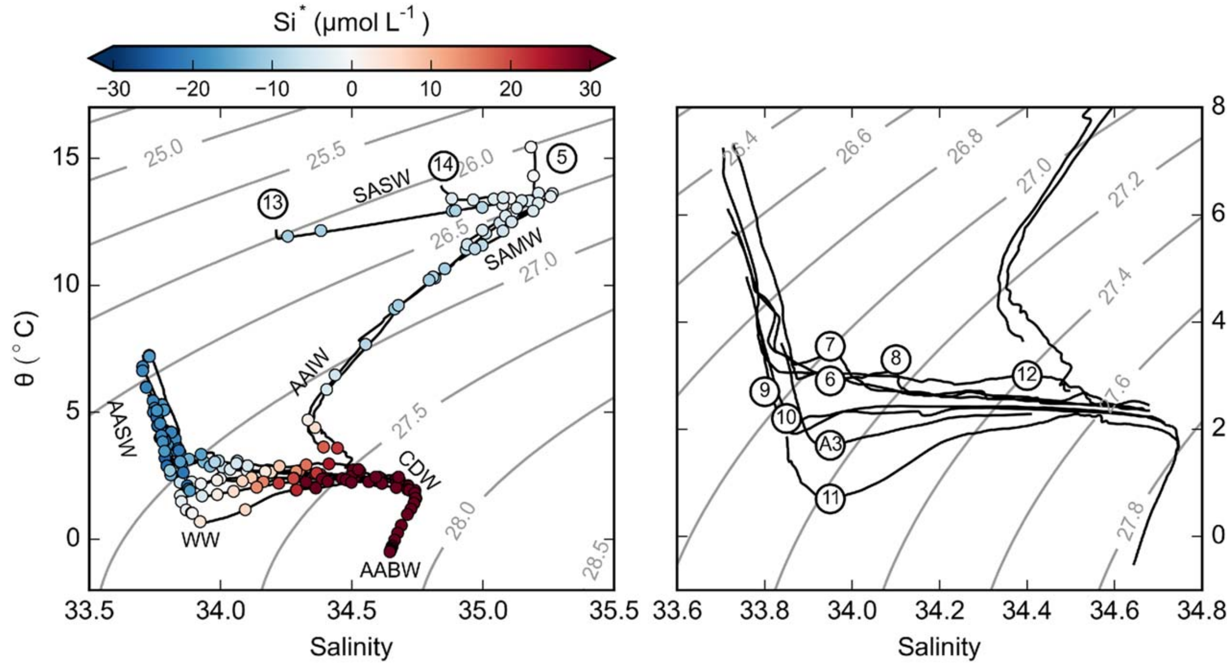

Fig. 2. Potential temperature/salinity diagram. (a) Colored points denote Si* ($Si(OH)_4 - NO_3^-$) distribution. Circled labels refer to stations. The main water masses identified are specified: SASW, Subantarctic Surface Water; SAMW, Subantarctic Mode Water; AAIW, Antarctic Intermediate Water; AASW, Antarctic Surface Water; WW, Winter Water; CDW, Circumpolar Deep Water; AABW, Antarctic Bottom Water. (b) Detailed view for stations of the PFZ and AAZ. [Color figure can be viewed in the online issue, which is available at wileyonlinelibrary.com.]

small and large diatoms that are thought to occupy different niches of nutrient and light availability, and have different sensitivity to grazing in the Southern Ocean (Smetacek et al. 2004; Quéguiner 2013). "Large diatoms (>100 μm)" comprised the following genera: *Corethron*, *Dactyliosolen*, *Membraneis*, *Pleurosigma*, *Proboscia*, *Rhizosolenia* and *Thalassiothrix*. "Small diatoms (<100 μm)" referred to the other diatom genera. Armored dinoflagellates (*Prorocentrum, Ceratium*, *Brachidinium*, *Dinophysis*, *Oxytoxum*, *Podolampas*, and *Protoperidinium)* were differentiated from naked dinoflagellates (*Gymnodinium* and *Gyrodinium*).

Results

Hydrological characteristics and nutrients diffusive flux

During the study (11 January to 08 February), the north Crozet bloom had terminated and partly advected by mesoscale features of the Subantarctic Front (SAF) associated with strong geostrophic velocities (Fig. 1). Surface waters of the PFZ displayed very low Chl *a* concentration (<0.3 μg L^{-1}) and the bloom of the central Kerguelen plateau was also declining (~0.8 μg L^{-1}). East of Kerguelen Island, on the northern flank of the PF, a Chl *a* plume originating from coastal waters was advected eastward as the PF merged with the SAF. A potential temperature-salinity diagram (Fig. 2) was used to classify the different stations into discrete hydrological zones, summarized in Table 1. The SAZ displayed the highest surface temperatures (>10°C, stations 5, 13, and 14). The PFZ exhibited a clear decrease in surface salinity (<34, stations 6, 7, 8, and 12) and the AAZ was characterized by the presence of a temperature minimum layer (~1.8°C; stations 9, 10, 11, and A3). The Si* (= $Si(OH)_4 - NO_3^-$) in intermediate and winter waters was homogeneous (~0 μmol L^{-1}) at all stations. Therefore, the Si* signature of surface waters was used as a tracer for $Si(OH)_4$ uptake relative to nitrate in the productive layer, rather than differences in preformed nutrients. In the SAZ, Si* was similar in surface water and intermediate waters (0 μmol L^{-1}) whereas in the PFZ and the AAZ, Si* in surface waters was strongly negative (<−20 μmol L^{-1}).

At all stations, 30–70% of the vertically integrated Chl *a* occurred deeper than the MLD (Table 2). However, only stations 6, 9, 12, 13, and 14 exhibited a maximum Chl *a* concentration deeper than the MLD. Brunt-Väisälä frequencies (*N*) were highest in the transition layer and ranged from 4.5 cycles h^{-1} to 8.2 cycles h^{-1}, with high values associated with frontal (e.g., station 13 close to SAF) or bathymetric (station 6 near the Crozet plateau) structures. At stations located close to the Kerguelen plateau (9, 10 and A3), Ze was shallower than the MLD. Station 9 displayed a characteristic subsurface chlorophyll maximum where Chl *a* shows a steep increase under the MLD (70 m) and a gradual decrease in the pycnocline down to 150 m (Fig. 3). Kz values peak at 9.5 $\times 10^{-5}$ m^2 s^{-1} in the mixed layer but display a second maximum associated with the pycnocline, nutriclines, and

Table 2. Sample code (M: mixed layer, T: transition layer, D: 250 m), sampling depth and concentrations of particulate organic carbon (POC), nitrogen (PON), and phosphorous (POP). Nutrient diffusive flux was calculated using a Kz value of 4.5×10^{-5} m^2 s^{-1} in the transition layer (see materials and methods).

Sample	Depth (m)	Particulate stock (μmol L^{-1})				Chlorophyll *a* (μg L^{-1})	Nutrient gradient (μmol m^{-4})			Nutrient diffusive flux (μmol m^{-2} d^{-1})			Brunt-Väisälä Frequency (cycle h^{-1})
		POC	PON	POP	BSi		$Si(OH)_4$	NO_3^-	PO_4^{3-}	$Si(OH)_4$	NO_3^-	PO_4^{3-}	
5M	20	18.60	2.34	0.19	1.07	1.26	0	78	7	—	—	—	3.1
5T	57	3.30	0.47	0.06	0.25	0.20	46	94	1	178	367	6	4.8
5D	250	1.10	0.15	0.02	0.02	0.01	15	35	2	—	—	—	2.3
6M	30	6.00	0.93	0.09	0.17	0.50	0	20	1	—	—	—	2.7
6T	71	5.53	0.85	0.05	0.25	0.67	100	89	7	390	345	25	8.2
6D	250	1.48	0.18	0.02	0.19	0.02	133	37	2	—	—	—	2.5
7M	39	4.85	0.72	0.10	0.16	0.40	37	0	4	—	—	—	2.9
7T	74	2.66	0.41	0.02	0.20	0.41	108	61	2	419	236	8	6.5
7D	249	1.27	0.18	0.02	0.17	0.02	81	20	2	—	—	—	2.2
8M	32	4.56	0.64	0.08	0.10	0.73	18	0	5	—	—	—	1.9
8T	100	4.93	0.80	0.04	0.26	0.37	69	49	3	269	191	10	5.1
8D	250	1.29	0.13	0.02	0.18	0.02	107	15	2	—	—	—	2.8
9M	50	7.25	1.10	0.17	3.19	0.83	27	8	0	—	—	—	2.2
9T	110	5.01	0.73	0.09	4.35	1.04	241	22	4	935	86	16	6.9
9D	250	1.36	0.18	0.02	1.02	0.04	168	37	3	—	—	—	2.9
10M	49	7.79	1.09	0.15	4.91	1.00	12	0	1	—	—	—	2.1
10T	99	3.45	0.42	0.06	3.14	0.69	342	71	6	1328	274	24	5.8
10D	248	1.36	0.17	0.02	0.57	0.03	156	19	2	—	—	—	2.4
11M	49	4.14	0.59	0.15	1.84	0.51	25	31	2	—	—	—	2.7
11T	119	3.46	0.43	0.09	1.52	0.63	143	15	3	556	58	10	4.4
11D	250	0.97	0.10	0.02	0.53	0.03	163	22	1	—	—	—	2.1
12M	40	4.57	0.62	0.07	0.24	0.49	21	18	0	—	—	—	3.3
12T	70	2.96	0.41	0.06	0.29	0.55	64	35	4	250	135	15	6.5
12D	250	1.46	0.15	0.02	0.21	0.03	109	40	1	—	—	—	2.6
13M	21	10.60	1.52	0.13	0.28	0.73	0	0	0	—	—	—	3.4
13T	46	6.77	0.95	0.08	0.37	0.82	71	24	0	277	93	0	8.2
13D	251	1.90	0.25	0.04	0.09	0.02	14	27	1	—	—	—	2.1
14M	20	10.49	1.59	0.15	0.33	0.62	0	0	3	—	—	—	4.1
14T	55	6.81	1.04	0.10	0.65	0.94	64	34	2	251	133	7	6.3
14D	250	1.85	0.20	0.03	0.09	0.04	2	22	1	—	—	—	2.1
A3M	41	9.36	1.47	0.25	4.71	1.10	1	15	0	—	—	—	2.0
A3T	110	8.19	1.31	0.18	5.08	1.20	426	83	6	1655	322	22	6.1
A3D	250	3.39	0.54	0.06	1.50	0.21	142	19	3	—	—	—	2.3

elevated Chl *a* values of 1.1 μg L^{-1}. The gradient between 150 m and the mixed layer was much higher for $Si(OH)_4$ (20 μmol L^{-1} to <2 μmol L^{-1}) than for NO_3^- (27 μmol L^{-1} to 23 μmol L^{-1}) and PO_4^{3-} (2.2 μmol L^{-1} to 1.5 μmol L^{-1}).

Nutrient gradients estimated for the three different layers covered two order of magnitude and were generally larger for $Si(OH)_4$ (Table 2). Highest $Si(OH)_4$ gradients (>200 μmol m^{-4}) were observed in the transition layer in stations of the AAZ close to the Kerguelen plateau (stations 9, 10, A3), leading to large $Si(OH)_4$ diffusive fluxes ($\geq$ 1 mmol m^{-2} d^{-1}). Highest NO_3^- gradients ($\sim$100 μmol m^{-4}) were found in the transition layer of stations 5 and 6 close to the Crozet Island, associated with the highest NO_3^- diffusive fluxes (>300 μmol m^{-2} d^{-1}). PO_4^{3-} gradients were at least one order of magnitude lower (<10 μmol m^{-4}) than nitrate gradient, resulting in negligible diffusive fluxes.

Particulate matter stocks and stoichiometry

POC concentrations generally decreased with depth with highest values found in the mixed layer of the SAZ (>10 μmol L^{-1}), followed by the AAZ (4.4–9.1 μmol L^{-1}) and PFZ (4.5–6.0 μmol L^{-1}, Table 2). The largest value of 18.6 μmol L^{-1} at station 5 corresponded to a biomass patch in a meander of the SAF (Fig. 1). POC concentrations in the transition

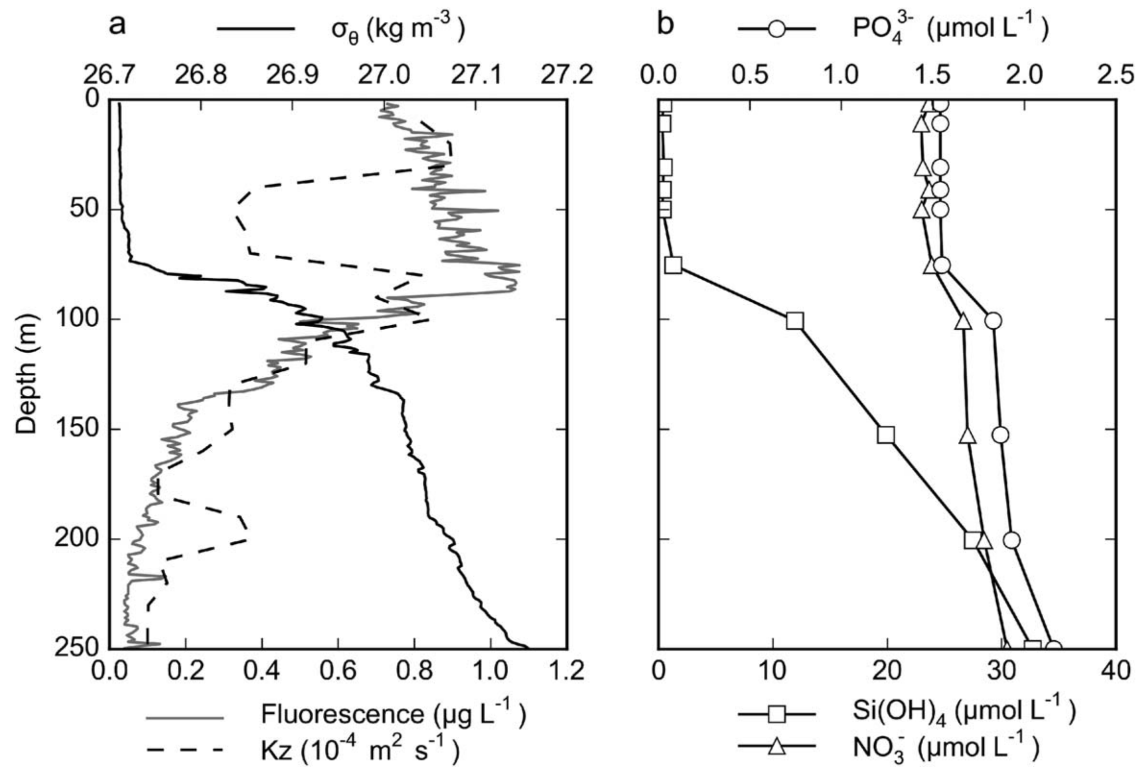

Fig. 3. Example of vertical profiles for station 9. (a) Potential density anomaly (σ_θ, black line), fluorescence-derived chlorophyll *a* (grey line) and turbulent diffusion coefficient (Kz, black dashed line). (b) Vertical profile of nitrate (triangles), phosphate (circles) and silicate (square).

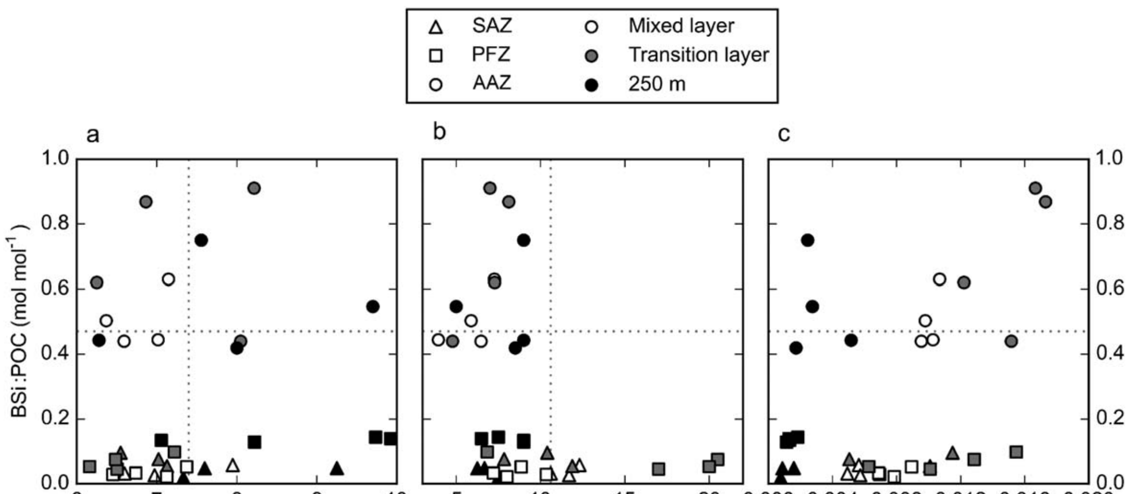

Fig. 4. Particulate matter stoichiometry. (a) POC:PON vs. BSi:POC. (b) PON:POP vs. BSi:POC. (c) Chl:POC vs. BSi:POC. Horizontal dashed line is the mean BSi:POC ratio from Quéguiner and Brzezinski (2002) for the Polar Frontal Zone in the Indian sector of the Southern Ocean (0.47). Vertical dashed line are the mean POC:PON and PON:POP ratios for the Southern Ocean from Martiny et al. (2013) (7.4 and 10.6, respectively).

layer ranged from 2.7 μmol L^{-1} to 8.2 μmol L^{-1} with the highest value observed over the Kerguelen plateau (Station A3). At the reference depth of 250 m POC concentrations were relatively uniform (1.4 ± 0.3 μmol L^{-1}), although on the Kerguelen plateau (Station A3) they were notably higher (3.4 μmol L^{-1}).

Table 3. Total microplankton cells abundances, total microplankton POC, and relative contribution of each microplanktonic group to the total abundance.

Sample	Total cell abundance (10^3 L^{-1})	Total micro-plankton POC (μmol L^{-1})	Contribution to total microplankton abundance (%)												
			Empty diatoms (>100 μm)	Empty diatoms (<100 μm)	Full diatoms (>100 μm)	Full diatoms (<100 μm)	CRS	Naked dinoflagellate	*Prorocentrum*	Other armored dinoflagellates	Naked ciliates	Tintinnids	Total diatoms	Total dinoflagellates	Total ciliates
5M	527	13.50	0	2	0	90	0	1	5	0	2	0	92	6	2
5T	25	1.34	1	3	1	60	0	4	25	1	4	1	65	30	5
5D	3	0.19	0	0	0	0	0	5	60	2	34	0	0	66	34
6M	49	3.23	0	5	1	19	0	9	38	0	28	1	24	47	28
6T	40	2.34	0	5	1	23	0	6	41	0	23	1	30	46	24
6D	5	0.16	0	48	0	4	0	3	33	1	11	0	52	37	11
7M	5	1.83	0	4	2	20	0	14	36	0	25	0	25	50	25
7T	8	1.26	0	22	2	20	0	6	34	0	15	0	45	40	15
7D	8	0.13	0	52	0	4	0	3	29	1	12	0	56	32	12
8M	12	2.29	0	1	1	17	0	24	24	0	33	0	19	49	33
8T	10	2.07	0	29	1	23	0	5	28	0	14	0	53	32	15
8D	6	0.14	0	15	0	0	0	5	59	1	20	0	15	65	20
9M	89	4.46	1	19	6	57	0	7	7	0	3	0	83	14	3
9T	104	3.41	1	32	3	51	0	4	6	0	2	0	87	10	2
9D	12	0.19	2	50	0	18	0	12	15	0	3	0	70	27	3
10M	145	4.38	1	18	7	67	0	4	3	0	1	0	92	7	1
10T	77	2.36	2	44	7	34	0	5	6	1	2	0	86	11	2
10D	11	0.11	0	38	0	1	0	16	18	0	26	0	39	34	26
11M	114	2.82	1	17	4	71	0	2	1	0	2	0	94	4	2
11T	75	1.50	1	52	2	33	0	5	4	0	2	0	89	9	2
11D	22	0.14	2	82	0	1	0	8	8	0	0	0	84	16	0
12M	24	2.28	0	15	12	35	0	5	28	0	5	1	61	33	5
12T	16	1.24	0	16	5	28	0	3	32	0	16	0	49	35	16
12D	13	0.14	3	63	1	8	0	1	18	0	6	0	75	19	6
13M	149	6.72	0	4	1	24	0	21	39	1	9	0	30	61	9
13T	77	4.31	0	3	1	48	0	9	26	4	8	0	53	39	8
13D	2	0.23	0	0	0	0	0	17	78	0	6	0	0	94	6
14M	103	6.15	1	0	4	23	0	12	42	7	11	1	28	61	12
14T	72	3.50	1	3	8	63	0	10	15	0	0	0	74	26	0
14D	4	0.13	1	5	2	4	0	18	68	1	1	1	12	87	2
A3M	108	7.29	2	17	13	60	0	3	3	1	2	0	91	7	2
A3T	234	5.75	0	13	8	66	8	1	2	0	1	0	95	3	2
A3D	110	2.89	1	17	0	37	39	2	2	0	1	0	94	4	1

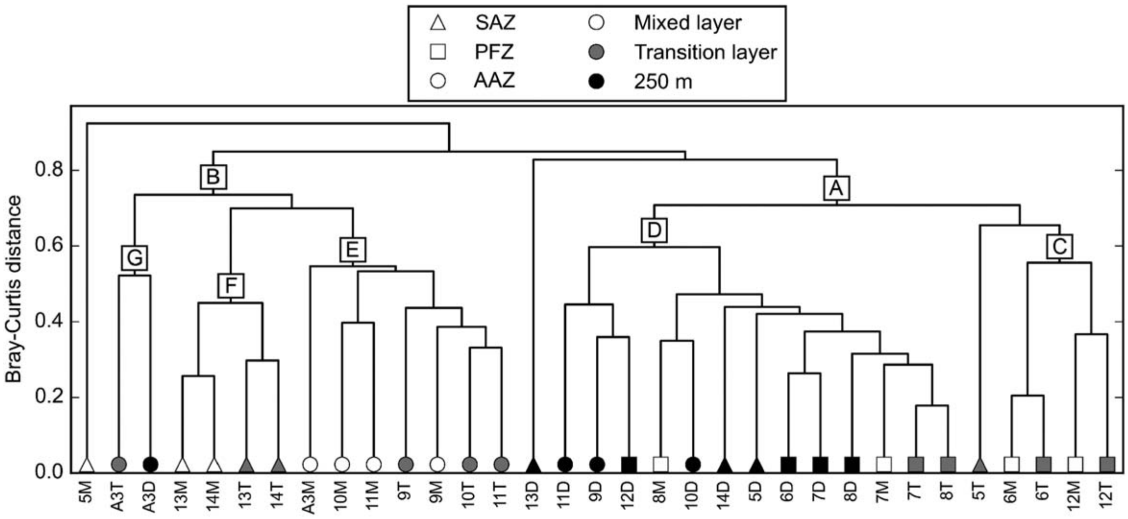

Fig. 5. Dendrogram of the hierarchical clustering (UPGMA agglomeration) based on the Bray-Curtis distance calculated on raw microplankton abundances. Capital letters categorize the groups referred to in the text.

The highest Chl *a* concentration was observed in the warm mixed layer of station 5 (1.26 μg L^{-1}). Stations in the PFZ exhibited the lowest mixed layer Chl *a* concentrations (0.40–0.50 μg L^{-1}), intermediate values were found in the SAZ (0.60–0.90 μg L^{-1}) and highest values in the AAZ ($\sim$1 μg L^{-1}). Unlike POC, Chl *a* values in the transition layer frequently exceeded those in the mixed layer, with the largest value of 1.20 μg L^{-1} observed at the Kerguelen plateau station A3. Similarly the largest 250 m Chl *a* concentration of 0.21 μg L^{-1} was observed at station A3, compared to negligible values of < 0.05 μg L^{-1} at all other stations.

All the samples from the SAZ and PFZ displayed BSi:POC ratios < 0.2 (Fig. 4). Conversely, in the AAZ, BSi:POC values were between 0.4 and 0.9 with highest values found in the transition layers. POC:PON ratios generally displayed a typical increase with depth with a notable exception at station A3 (Kerguelen plateau) where the POC:PON ratio was vertically homogeneous (6.3). PON:POP ratios demonstrated more variability than POC:PON. In the AAZ, PON:POP mixed layer ratios were between 4 and 8, increasing with depth. Mixed layer values in the PFZ (stations 6–10) were slightly higher than the AAZ (6–9), and SAZ samples were notably larger with values > 10. The highest values of 16–21 were found in transition layer PFZ samples located between the Crozet and Kerguelen Islands (stations 6, 7, and 8). Chl:POC ratio (g g^{-1}) were generally highest in the transition layer and lowest in 250 m samples. The largest Chl:POC ratios of 0.016–0.018 were observed in the transition layer of the AAZ.

Microplankton abundance and distribution

The largest microplankton cell abundance (527 $\times$ 10^3 cell L^{-1}) was observed in the mixed layer of station 5 and corresponded to a community dominated (>90%) by *Bacteriastrum* spp. (Table 3), constituting the external branch of the dendrogram based on Bray-Curtis distance (Fig. 5). The low biomass group A (<50 $\times$ 10^3 cell L^{-1}) contained the subgroup C which represented mixed layer and transition layer of PFZ stations 6 and 12 characterized by an equal proportion of full diatoms (>100 μm), *Prorocentrum* and naked ciliates. Subgroup D contained all of the 250 m samples (except A3) and transition layer samples from the PFZ stations 7 and 8, the latter characterized in decreasing order by empty diatoms (<100 μm), *Prorocentrum* and naked ciliates. Group B (high abundance) contained three subgroups, E, F, and G. Subgroup E represented the majority of surface and transition layer samples from the AAZ and was characterized by a strict dominance of full diatoms (<100 μm). Subgroup F constituted samples from the mixed and transition layer of SAZ stations 13 and 14 with an assemblage of *Prorocentrum* and full diatoms (<100 μm). Finally, subgroup G contained samples from the transition layer and deep layer at A3 dominated by CRS and full diatoms (<100 μm). It is generally stated that bottle sampling might under-sample large and rare diatoms (Armand et al. 2008). Therefore our data might underestimate the contribution of large diatoms to the total microplankton assemblage.

The fraction of empty diatoms generally increased with depth (up to 90% at 250 m in the PFZ), with the notable exception of station A3 where it remained $\sim$20%. *Fragilariopsis kerguelensis* dominated (>60%) the empty diatoms in all the samples of the AAZ and PFZ at any depth, with the exception of station A3 (Fig. 6). Station 5 was mostly characterized by empty *Bacteriastrum* spp. cells. In stations 13 and 14 (SAZ) the mixed layer empty diatom community was dominated by *Pseudo-nitzschia* spp., *Thalassiothrix antarctica* and *Chaetoceros Hyalochaete* (vegetative). Mixed layer sample

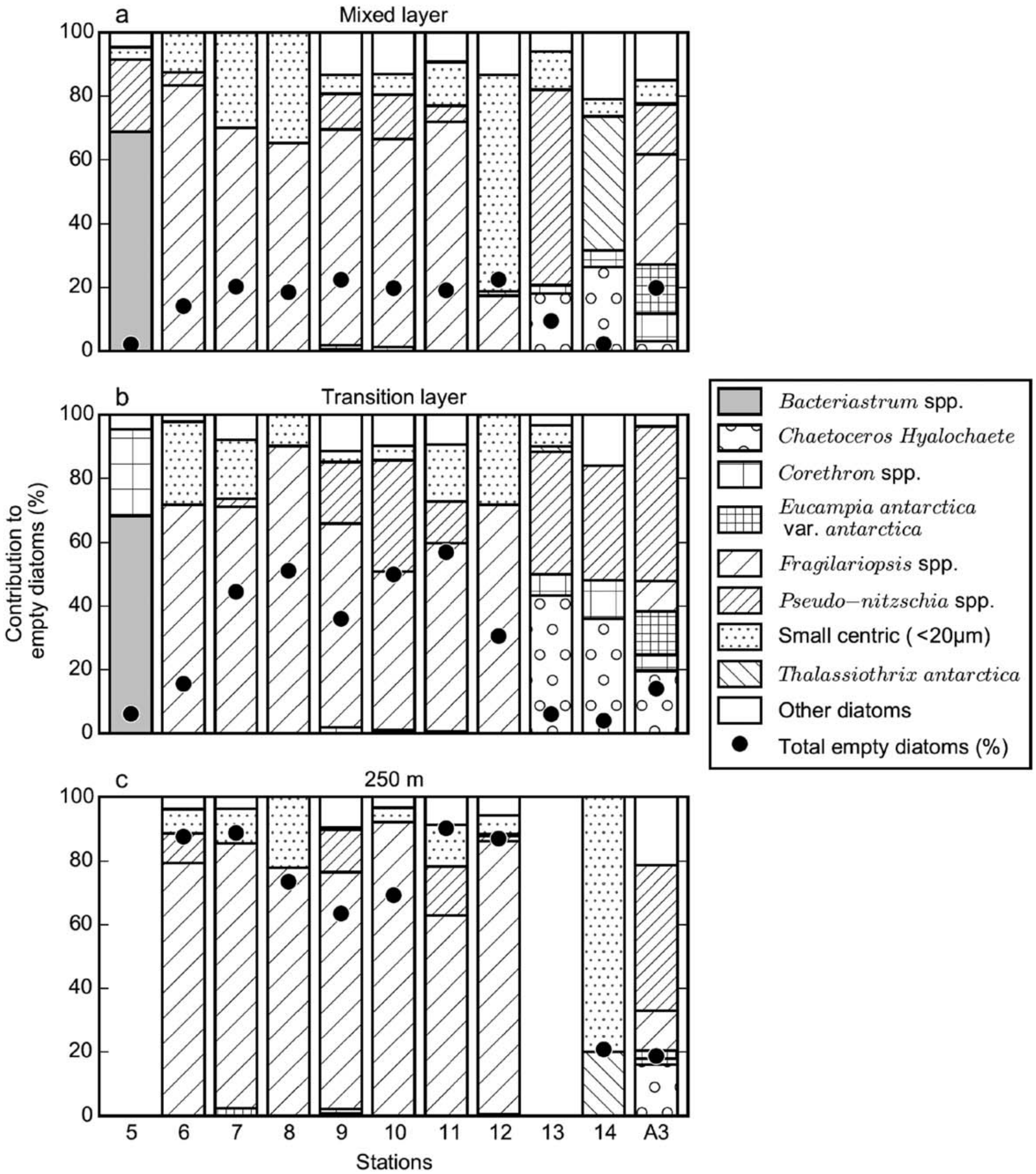

Fig. 6. Fraction of empty diatoms for (a) mixed layer samples, (b) transition layer samples, and (c) 250 m samples. Black dots represent the fraction of total empty diatoms to the sum of full and empty diatom frustules. Patterned bars refer to the fraction of a diatom group as specified in the legend.

at A3 contained in decreasing abundance empty cells of *F. kerguelensis*, *Pseudo-nitzschia* spp., *Eucampia antarctica* var. *antarctica* and *Corethron* spp. In the transition layer of stations 13 and 14 (SAZ), empty diatoms were dominated by *C. Hyalochaete* (vegetative) and *Pseudo-nitzschia* spp. At A3, empty diatoms in the transition layer were dominated by *Pseudo-nitzschia* spp. (50%), followed by *C. Hyalochaete* (vegetative) and *E. antarctica* var. *antarctica*. Finally, empty *Pseudo-nitzschia* (45%), *C. Hyalochaete* (vegetative, 18%) and *F. kerguelensis* (12%) were observed at 250 m at A3.

Microplankton POC partitioning

A highly significant linear correlation (Spearman, $n = 33$, $\rho = 0.88$, $p < 0.01$) was found between the measured POC (Table 2) and the calculated total microplankton POC (POC_{micro}, Table 3). The regression slope (0.7), and significant intercept ($\sim$1 μmol L^{-1}), suggested that the microplankton biomass calculation underestimated the total POC. At station 5, the mixed layer sample was dominated by *Bacteriastrum* spp. (>60%, Fig. 7). At stations 6 to 8 (PFZ between Crozet and Kerguelen), naked ciliates (>40%) and dinoflagellates

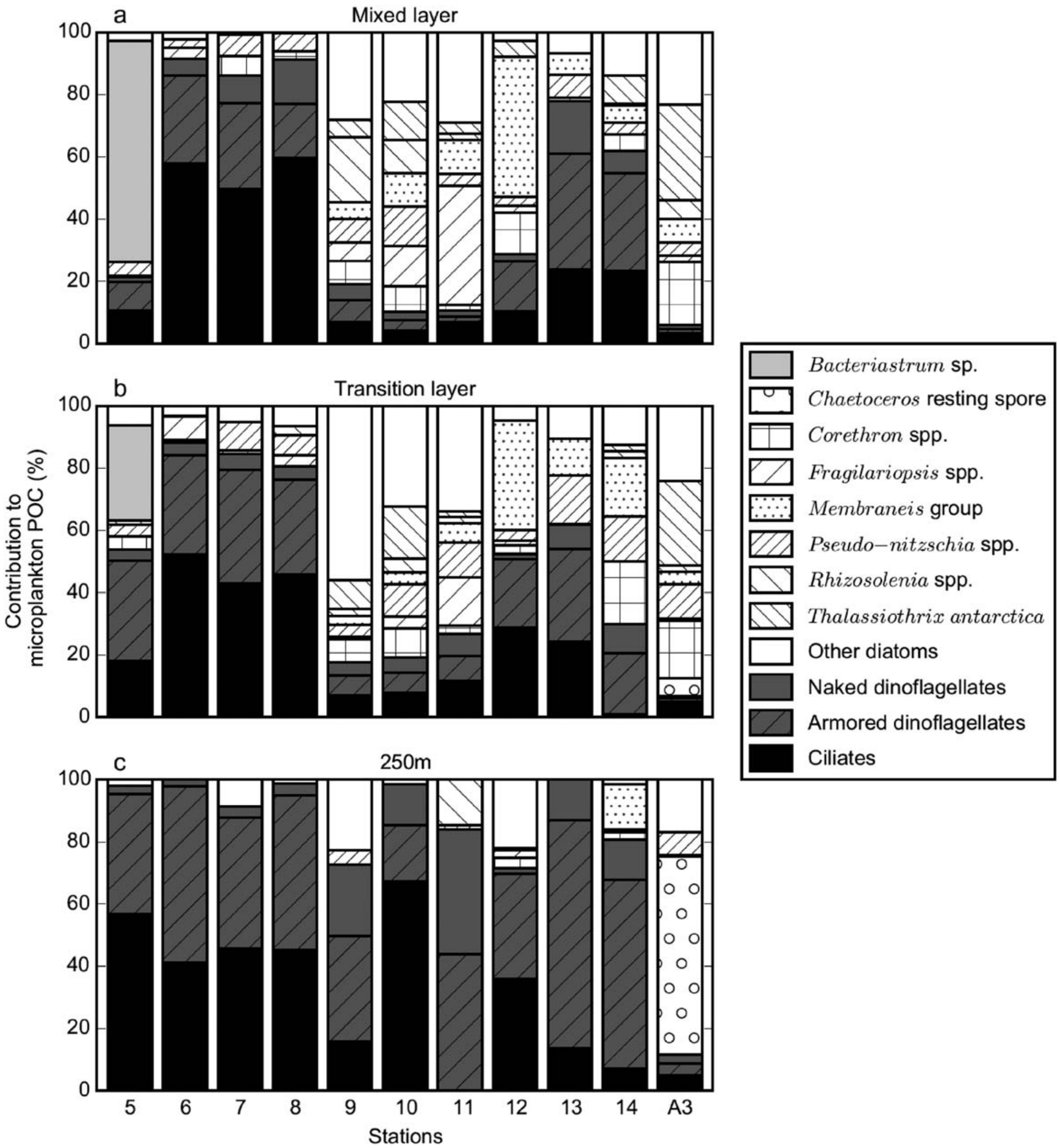

Fig. 7. Microplankton POC partitioning for (a) mixed layer samples, (b) transition layer samples, and (c) 250 m samples. Patterned bars refer to the contribution of a microplankton group as specified in the legend.

were the main contributors to POC_{micro} at any depth. In the mixed layer samples of stations 13 and 14 (SAZ) dinoflagellates dominated (>50%) the POC_{micro}. In the AAZ, diatoms dominated POC_{micro} at all stations, with a major contribution of the assemblage of large diatoms (>100 μm): *Rhizosolenia* spp., *Corethron* spp., *T. antarctica, Membraneis* and *F. kerguelensis* (<100 μm). The same pattern of dominant taxa was also observed in the transition layer of the AAZ. At stations 12, 13, and 14 (north of Kerguelen), dinoflagellates followed by *Membraneis* and *Pseudo-nitzschia* spp. were the main contributors to POC_{micro}. In the deep samples, POC_{micro} was dominated by the contribution of dinoflagellates (mainly *Prorocentrum*) and ciliate biomass with a noticeable exception at station A3 with the presence of *C. Hyalochaete* resting spores (>60% POC_{micro}).

Particulate matter signature and microplankton assemblages

The first two axes of the CCA accounted for ~88% of the variability within the dataset (Fig. 8). Axis 1 opposed AAZ and SAZ stations characterized by a dominance of diatoms and high BSi:POC stoichiometry to the PFZ stations dominated by dinoflagellates and ciliates and a high PON:POP ratio. Axis 2 globally opposed surface samples with marked

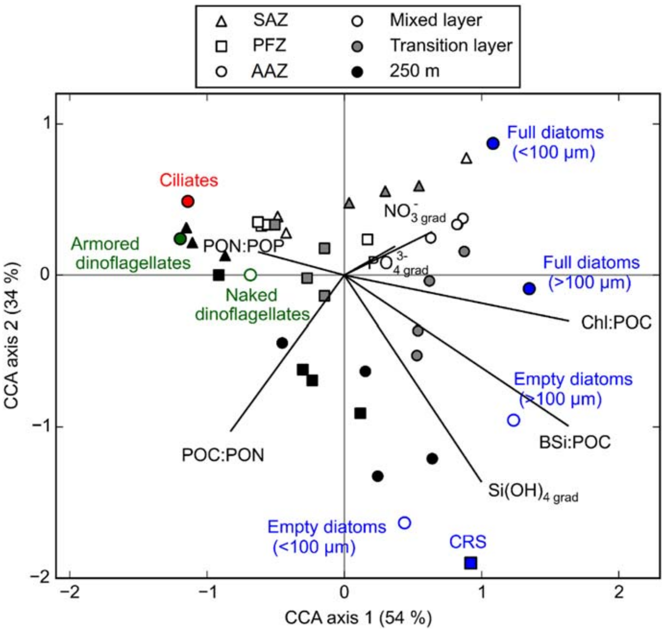

Fig. 8. Projection of samples, main microplankton groups and biogeochemical factors (particulate matter stoichiometry and major nutrients diffusive fluxes) on the first two axes of the canonical correspondence analysis (CCA). [Color figure can be viewed in the online issue, which is available at wileyonlinelibrary.com.]

NO_3^- and PO_4^{3-} gradients associated with full diatoms (<100 μm) to the 250 m samples with a high POC:PON ratio associated with empty diatoms (<100 μm). Full diatoms (>100 μm) were projected close to the Chl:POC ratio and the AAZ transition layer samples. Finally, empty diatoms (>100 μm) were projected close to the $Si(OH)_4$ gradient, the BSi:POC ratio and the transition layer samples and deep samples of the AAZ.

Discussion

Microplankton community and physiology in the transition layer

During our study (January–February), the period of maximum productivity had already occurred (Supporting Information animation). The North Crozet bloom ended and was partly advected eastward in the SAF, and the central Kerguelen plateau bloom was also in decline. Large and negative Si* values in the PFZ and AAZ (Fig. 2) suggested intense $Si(OH)_4$ utilization compared to nitrate utilization associated to bloom features. This can result from a dominance of diatoms in phytoplankton populations together with an increase in Si:N uptake ratio in response to iron limitation (Hutchins and Bruland 1998; Takeda 1998; Moore et al. 2007). Low concentrations of $Si(OH)_4$ (1.8 μmol L^{-1}; Mosseri et al. 2008) and dissolved iron (~0.1 nmol L^{-1}; Blain et al. 2008) over the central Kerguelen plateau in summer suggest that both elements may limit diatom growth in summer mixed layers.

The subsurface chlorophyll maximum is a recurrent feature in the oligotrophic ocean (Venrick et al. 1973; Letelier et al. 2004; Mignot et al. 2014), the North Sea (Weston et al. 2005), and the Arctic (Martin et al. 2010). The SCM can be associated with a phytoplankton biomass maximum (Martin et al. 2010), or the two structures can be uncoupled, suggesting that the vertical distribution of chlorophyll is strongly determined by photoacclimation (Fennel and Boss 2003). In the Southern Ocean, it has been proposed that the development of sub-surface biomass features is linked to such nutrient depletion, in particular iron in the mixed layer (Parslow et al. 2001). Under these conditions, phytoplankton accumulates in temperature minimum layers that are frequently associated to the pycnocline and/or nutricline (Holm-Hansen and Hewes 2004). In this study, a large fraction of integrated Chl *a* was observed below the mixed layer and the euphotic layer in the SAZ, PFZ and AAZ in the vicinity of the Crozet and Kerguelen plateaus. The transition layer constitutes a physical interface of increased water column stability, as diagnosed by maximum Brunt-Väisälä frequencies (Table 2). However, although POC and POC_{micro} concentrations were higher in the transition layer relative to the deep-reference samples, they were notably lower than those of the mixed layer (Tables 2, 3), not indicative of biomass accumulation on this physical interface. Furthermore, examples of significant sub-surface biomass accumulation in the Southern Ocean have been associated to divergent diatom communities with an accumulation of larger diatoms at depth (Kopczynska et al. 2001). In our regional survey, mixed layer and transition layer diatom communities were similar, consistent with more localised studies (Armand et al. 2008; Gomi et al. 2010). The data presented above suggests that subsurface chlorophyll features are not necessarily associated with biomass accumulation in the Southern ocean and this is consistent across a broad spatial scale.

In the PFZ and AAZ, the highest Chl:POC ratios were observed in the transition layer and we suggest this is linked to photoacclimation. It is known that Chl:POC ratios of phytoplankton can cover more than one order of magnitude (0.003–0.055 g g^{-1}; Cloern et al. 1995) and due to photoacclimation vary fourfold among single diatom species (Anning et al. 2000). The CCA results highlight the association of high Chl:POC ratios with full and large (>100 μm) diatom cells in the transition layer of the AAZ. Southern Ocean diatoms have developed an acclimation strategy to low light and iron levels by increasing the amount of light-harvesting pigments on photosynthetic units, rather than multiplying the number of photosynthetic units (Strzepek et al. 2012).

It has been suggested previously that nutrient diffusion through the pycnocline could sustain phytoplankton production in a transition layer when mixed layer nutrient concentrations reach limiting levels (Holm-Hansen and Hewes

2004; Johnston and Rudnick 2009; Quéguiner 2013). There was no evidence of oxygen accumulation in the transition layer (data not shown) suggesting minimal photosynthetic production, although diffusion and heterotrophic respiration may have dampened an already low signal. Unfortunately no carbon fixation data is available to validate the hypothesis of negligible photosynthetic rates below the euphotic layer. However, production in the transition layer would also require iron diffusion but ferriclines can be significantly deeper than mixed layers and transition layers. On the Kerguelen plateau, although the transition layer occurs at 110 m, the ferricline is located at 175 m in summer (Blain et al. 2008). This is a pattern generally applicable to the Southern Ocean as a whole, where summer ferricline horizons appear to be systematically deeper than MLDs (Tagliabue et al. 2014) and thus significant carbon fixation by transition layer communities appears unlikely. Our data suggests that sub-surface chlorophyll features can be attributed to photoacclimatation of mixed layer communities within the transition layer, rather than production and subsequent biomass accumulation at this interface.

Late summer transition layers as a site for carbon and silicon decoupling

We propose Southern Ocean transition layers as a key location in the water column where carbon and silicon elemental cycles are decoupled. A notable biogeochemical feature of late summer transition layers in our study region is elevated BSi:POC ratios compared to mixed layer samples (Fig. 4). In contrast to the deep water-column (250 m), mixed layer and transition layer diatom communities are quite similar. This indicates that differences in diatom community structure, (i.e., shifts to larger diatoms in sub-surface communities, Kopczynska et al. 2001) does not act as a major control in driving the patterns in BSi:POC ratios as a function of depth. In contrast, the proportion of empty diatom frustules in the transition layer is markedly increased compared to the mixed layer (Fig. 6). Specifically, we observed an accumulation of empty *F. kerguelensis* and *Pseudo-nitzschia* cells associated to high BSi:POC ratios. Programmed cell death, viral lysis and grazing pressure have all been proposed as mechanisms that could lead to the accumulation of empty frustules (Assmy et al. 2013). In this context, transition layers have been identified as grazing hotspots for micro- and meso-zooplankton (Holm-Hansen and Hewes 2004; Gomi et al. 2010). A high BSi:POC ratio is an inherent property to the iron-limited ACC characterized by the dominance of heavily silicified diatoms (Smetacek et al. 2004), our results suggest it might be enhanced within the transition layer transitional layer due to elevated heterotrophic activity and zooplankton grazing. Additionally, transition layers in the SAZ and at A3 displayed a low fraction of empty frustules and a high abundance of large *Corethron* spp. or very large *Thalassiothrix antarctica*. The large size of these diatom might confer them a resistance to grazing (Smetacek et al. 2004), resulting in a low proportion of empty frustules for these species.

In the AAZ, we observed high $Si(OH)_4$ diffusive fluxes in the transition layer, mainly driven by a strong $Si(OH)_4$ gradient generated by the intense silicon utilization by diatoms in surface waters in summer, and to a lesser extent by an increased Kz within the transition layer. Carbon fixation relies on iron-dependent photosynthesis whereas Si fixation depends on energy from respiration (Martin-Jézéquel et al. 2000) and may thus occur independent of light (Chisholm et al. 1978; Martin-Jézéquel et al. 2000). Silicification may be sustained by vertical diffusion of $Si(OH)_4$ (Table 2) and, even at low levels, may partly contribute to the increase in BSi:POC ratios in AAZ transition layers. Consequently the transition layer may represent a location in the water column where carbon and silicon fixation can become physiologically decoupled, although direct measurements of carbon and silicon uptake (e.g., Closset et al. 2014) would be necessary to confirm this hypothesis.

Regional patterns in microplankton diversity and particulate matter stoichiometry

The hierarchical clustering and the CCA suggest strong regional patterns in microplankton community structure relative to the frontal location and the depth. The dominance of the sub-tropical diatom *Bacteriastrum* in the warm surface water waters (15°C) in the SAZ is likely to result from the southward advection of a the Subtropical Front meander. In general mixed layer communities in the SAZ and PFZ were dominated by the dinoflagellate *Prorocentrum*, in terms of both abundance and biomass. A major contribution of dinoflagellates to late summer phytoplankton biomass was also observed in the SAZ of the Crozet Basin (Kopczyńska and Fiala 2003), although flagellates and coccolithophorids dominated the numerical assemblage (Fiala et al. 2004), consistent with the regional pattern of coccolith sedimentation (Salter et al. 2014). Poulton et al. (2007) reported that post-bloom phytoplankton communities in the PFZ, North of the Crozet plateau, were dominated by the nanoplanktonic *Phaeocystis antarctica*, with a low contribution by the small diatom *Thalassionema nitzschioides*. The low contribution of diatoms to late summer biomass in the mixed layer of the SAZ and PFZ is consistent with the commonly observed succession of diatoms to dinoflagellates from spring to summer (Margalef 1978; Barton et al. 2013). Ciliates significantly contributed to phytoplankton biomass in the mixed layer of the PFZ, indicative of nutrient limitation driving a switch towards a more heterotrophic food-web as often observed at a global scale (Margalef 1958; Landry and Calbet 2004) and during artificial (Gall et al. 2001; Henjes et al. 2007) and natural (Poulton et al. 2007) iron-fertilization studies in the Southern Ocean.

In contrast to the patterns described above, diatoms still heavily dominated AAZ microplankton communities at the time of sampling (>80% abundance, > 70% biomass), notably through the contribution of large diatoms such as *Membraneis*, *Corethron* and *Rhizosolenia*. A dominance of the large diatom *Corethron pennatum* to the total biomass was previoulsy reported in late summer in the AAZ south of Crozet Islands (Poulton et al. 2007). In the AAZ west of South Georgia, diatoms also dominate phytoplankton biomass in late summer with a strong contribution of *Pseudo-nitzschia*, *T. antarctica*, and *E. antarctica* var. *antarctica* (Korb and Whitehouse 2004; Korb et al. 2008, 2010). We observed a strong contribution of the very large diatom *Thalassiothrix antarctica* together with *Corethron* spp. to the total biomass at the central Kerguelen plateau station A3. This is consistent with previous observations at the same station in summer during KEOPS1, although in the latter *E. antarctica* dominated diatom biomass (Armand et al. 2008). On the Kerguelen plateau dinoflagellates contribution to biomass and abundance was lower (mainly though the representation of the genera *Gyrodinium* and *Prorocentrum*) and similar to observations made during KEOPS1 (>20% microplankton biomass; Sarthou et al. 2008). Over the Kerguelen plateau, diapycnal iron diffusive flux in summer (Blain et al. 2008; Chever et al. 2010) might sustain diatom production and explain why the microplankton community has not shifted to a dominance of dinoflagellates and ciliates.

Regional patterns in PON:POP stoichiometry of particulate matter were strongly correlated with the distribution of major microplankton groups across frontal zones and at different depth horizons. The CCA highlights the general association of elevated PON:POP ratios with dinoflagellates and ciliates. Furthermore, PON:POP ratios were lowest in the mixed layer of the AAZ (4–7) and transition layer of the AAZ (5–8) where biomass is dominated by diatoms (>70%). In culture, N:P ratios of ~10 for the dinoflagellates *Gymnodinium dominans* and *Oxyrhhis marina* and 10–15 for the ciliate *Euplotes* have been reported (Golz et al. 2015). Under optimal growth conditions *O. marina* exhibits high N:P ratios of 25 (Malzahn et al. 2010). Similarly several studies have reported low N:P ratio from diatom cultures (<10; Ho et al. 2003; Quigg et al. 2003). During the EIFEX artificial-iron fertilization experiment, *F. kerguelensis* was reported to grow with an N:P ratio of 3–4 (Hoffmann et al. 2007). During KEOPS2, N:P ratio of 6–15 was found in the high biomass stations of the PFZ east of Kerguelen Islands (Lasbleiz et al. 2014). In agreement with these previous studies, our results suggest that broad-scale shifts in microplankton community composition in the Southern Ocean can modulate particulate matter stoichiometry and are consistent with the major latitudinal trends observed globally (Martiny et al. 2013).

There are some notable subtleties to the general trends presented above. SAZ mixed layer particles exhibit relatively high PON:POP ratios (10–12) even if the community was dominated by diatoms (e.g., Station 5; > 75% *Bacteriastrum* sp.). Resource allocation in Southern Ocean diatoms is known to be highly sensitive to temperature with more P-rich ribosomes being required for protein synthesis under low temperature resulting in a lower N:P ratio (Toseland et al. 2013). Mixed layer waters of the SAZ are notably warmer (10–15°C) than the AAZ (2–4°C), which may result in higher PON:POP ratio for diatom-dominated communities of the SAZ compared to the AAZ. Iron-limitation is an additional plausible mechanism that may modulate PON:POP ratios. Iron limitation decreases nitrate uptake (Price et al. 1994) and nitrate reductase activity (Timmermans et al. 1994), leading to lower N:P ratio in iron-limited diatom cultures (Price 2005). Furthermore, Hoffmann et al. (2006) reported a strong N:P increase (4 to 16) in the > 20 μm fraction following iron addition in iron-limited cultures. The dissolved iron concentration is < 0.15 nmol L^{-1} in the mixed layer in the AAZ over the central Kerguelen plateau in February (Blain et al. 2008) and therefore iron limitation may have lowered PON:POP ratios observed in the diatom-dominated AAZ samples. In conclusion microplankton community structure appears to exert a first order control on PON:POP stoichiometry in late summer in this sector of the Southern Ocean. Physiological constraints linked to environmental factors, such as temperature and iron limitation, are also able to modulate this ratio.

Implications for carbon and silicon export

A recent compilation of carbon export estimates over the Kerguelen plateau (station A3) indicates a strong POC flux attenuation between the mixed layer and 300 m (Rembauville et al. 2015b). In this region we observed similarly high BSi:POC ratios in the transition layer (~0.8) compared to sediment trap samples (0.7–1.5) at the end of summer (Rembauville et al. 2015a). *F. kerguelensis* was mostly present in the form of empty frustules in the transition layer, consistent with its classification as a preferential "silica sinker" (Smetacek et al. 2004; Assmy et al. 2013) that has been confirmed by sediment trap studies (Salter et al. 2012; Rembauville et al. 2015a; Rigual-Hernández et al. 2015). In contrast, the large *Rhizosolenia* spp. (~500 μm) and very large *T. antarctica* (up to 3–4 mm) were present as full cells within the transition layer, an observation consistent with their recent quantification as a "carbon sinker" over the central Kerguelen plateau (Rembauville et al. 2015a). However, the large frustule of these species confers a resistance to grazing (e.g., Smetacek et al. 2004) and high Si:C ratio that may drive a significant contribution to silicon sinking.

It is generally stated that diatom-dominated ecosystems are more efficient in exporting carbon from the mixed layer compared to more recycling systems dominated by dinoflagellates and ciliates (Smetacek 1985; Legendre and Le Fèvre 1989; Boyd and Newton 1995, 1999; Legendre and Rivkin 2015). However, despite a dominance of diatoms in the mixed layer microplankton assemblage in the AAZ, the deep (250 m) POC concentrations in the AAZ were comparable to the PFZ and SAZ (0.9–1.36 μmol L^{-1} vs. 1.10–1.90 μmol L^{-1}) where dinoflagelates and ciliates dominated the microplankton assemblage. Although one must be cautious in equating standing stocks to fluxes these data suggest that in late summer in the Southern Ocean, a higher proportion of diatoms in the mixed layer does not consistently lead to a higher transfer of carbon at 250 m. Intense zooplankton grazing of diatom biomass in the transition layer, as evidenced by the increased proportion of empty cells relative to the mixed layer, presumably results in the efficient consumption and recycling of exportable biomass reducing diatom-mediated carbon transfer into the ocean interior. This has been suggested previously as an explanation for High biomass Low Export Environments (Lam and Bishop 2007; Lam et al. 2011; Jacquet et al. 2011). Moreover, a strong response of heterotrophic microbial communities to the high primary production levels (Obernosterer et al. 2008) and the association of specific bacterial communities with deep biomass features (Obernosterer et al. 2011) might also strongly contribute to the remineralization of POC over the Kerguelen plateau. An efficient response of both microbial and mesozooplanktonic communities to POC availability is consistent with the inverse relationship between diatom-dominated primary production and export efficiency observed in the Southern Ocean (Maiti et al. 2013). Furthermore we observed a progressive increase of diatoms present as empty frustules through the water column and a significantly higher contribution of dinoflagellates and ciliates to total microplankton POC at 250 m compared to the transition layer. These data show the importance of zooplankton grazing in modulating diatom export production during late summer Southern Ocean ecosystems and highlight the potential importance of ciliates and dinoflagellates to the biological carbon pump at these specific times.

A notable exception to the patterns described above are the observations from station A3, on the Kerguelen plateau, where deep microplankton POC is dominated by *Chaetoceros Hyalochaete* resting spores (80%), leading to POC concentrations that are ~3 times higher than mean values at 250 m in the AAZ, PFZ and SAZ. This observation is broadly consistent with a recent sediment trap study which documented *C. Hyalochaete* resting spores as the dominant contributor to the annual carbon export (>60%) mediated through two rapid flux events occurring at the end of summer (Rembauville et al. 2015a). If the transition layer is a place of intense grazing pressure then our results consolidate the idea that resting spores are a specific ecological vector for carbon export through intense remineralization horizons. Indeed, small and highly silicified CRS have been demonstrated to lower copepod grazing pressure in culture (Kuwata and Tsuda 2005). In line with recent sediment trap results, the present study supports the pivotal role of diatom resting spores for carbon export from natural iron fertilized blooms in the Southern Ocean (Salter et al. 2007, 2012; Rembauville et al. 2015a). The net impact of diatom-dominated communities on carbon export strongly depends on the ecology of the species present. Preferential silicon sinking species poorly contribute to carbon export contrary to carbon sinking species, such as diatoms that form resting spores. A coupled description of mixed layer properties (nutrient dynamics and phytoplankton communities) and export out of the mixed layer over an entire productive cycle remains necessary to better understand processes responsible for resting spore formation.

References

Aminot, A., and R. Kerouel. 2007. Dosage automatique des nutriments dans les eaux marines: Méthodes en flux continu. Ifremer.

Anning, T., H. L. MacIntyre, S. M. Pratt, P. J. Sammes, S. Gibb, and R. J. Geider. 2000. Photoacclimation in the marine diatom *Skeletonema costatum*. Limnol. Oceanogr. **45**: 1807–1817. doi:10.4319/lo.2000.45.8.1807

Armand, L. K., V. Cornet-Barthaux, J. Mosseri, and B. Quéguiner. 2008. Late summer diatom biomass and community structure on and around the naturally iron-fertilised Kerguelen Plateau in the Southern Ocean. Deep Sea Res. Part II Top. Stud. Oceanogr. **55**: 653–676. doi:10.1016/j.dsr2.2007.12.031

Assmy, P., and others. 2013. Thick-shelled, grazer-protected diatoms decouple ocean carbon and silicon cycles in the iron-limited Antarctic Circumpolar Current. Proc. Natl. Acad. Sci. U. S. A. **110**: 20633–20638. doi:10.1073/pnas.1309345110

Barton, A. D., Z. V. Finkel, B. A. Ward, D. G. Johns, and M. J. Follows. 2013. On the roles of cell size and trophic strategy in North Atlantic diatom and dinoflagellate communities. Limnol. Oceanogr. **58**: 254–266. doi:10.4319/lo.2013.58.1.0254

Blain, S., and others. 2001. A biogeochemical study of the island mass effect in the context of the iron hypothesis: Kerguelen Islands, Southern Ocean. Deep Sea Res. Part I Oceanogr. Res. Pap. **48**: 163–187. doi:10.1016/S0967-0637(00)00047-9

Blain, S., G. Sarthou, and P. Laan. 2008. Distribution of dissolved iron during the natural iron-fertilization experiment KEOPS (Kerguelen Plateau, Southern Ocean). Deep Sea Res. Part II Top. Stud. Oceanogr. **55**: 594–605. doi:10.1016/j.dsr2.2007.12.028

Borrione, I., and R. Schlitzer. 2013. Distribution and recurrence of phytoplankton blooms around South Georgia, Southern Ocean. Biogeosciences **10**: 217–231. doi:10.5194/bg-10-217-2013

Boyd, P., and P. Newton. 1995. Evidence of the potential influence of planktonic community structure on the interannual variability of particulate organic carbon flux. Deep Sea Res. Part I Oceanogr. Res. Pap. **42**: 619–639. doi:10.1016/0967-0637(95)00017-Z

Boyd, P. W., and P. P. Newton. 1999. Does planktonic community structure determine downward particulate organic carbon flux in different oceanic provinces? Deep Sea Res. Part I Oceanogr. Res. Pap. **46**: 63–91. doi:10.1016/S0967-0637(98)00066-1

Chever, F., G. Sarthou, E. Bucciarelli, S. Blain, and A. R. Bowie. 2010. An iron budget during the natural iron fertilisation experiment KEOPS (Kerguelen Islands, Southern Ocean). Biogeosciences **7**: 455–468. doi:10.5194/bg-7-455-2010

Chisholm, S. W., F. Azam, and R. W. Eppley. 1978. Silicic acid incorporation in marine diatoms on light:dark cycles: Use as an assay for phased cell division 1. Limnol. Oceanogr. **23**: 518–529. doi:10.4319/lo.1978.23.3.0518

Cloern, J. E., C. Grenz, and L. Vidergar-Lucas. 1995. An empirical model of the phytoplankton chlorophyll : Carbon ratio-the conversion factor between productivity and growth rate. Limnol. Oceanogr. **40**: 1313–1321. doi:10.4319/lo.1995.40.7.1313

Closset, I., and others. 2014. Seasonal evolution of net and regenerated silica production around a natural Fe-fertilized area in the Southern Ocean estimated with Si isotopic approaches. Biogeosciences **11**: 5827–5846. doi:10.5194/bg-11-5827-2014

Cornet-Barthaux, V., L. Armand, and B. Quéguiner. 2007. Biovolume and biomass estimates of key diatoms in the Southern Ocean. Aquat. Microb. Ecol. **48**: 295–308. doi:10.3354/ame048295

de Baar, H. J. W., A. G. J. Buma, R. F. Nolting, G. C. Cadée, G. Jacques, and P. Tréguer. 1990. On iron limitation of the Southern Ocean: Experimental observations in the Weddell and Scotia Seas. Mar. Ecol. Prog. Ser. **65**: 105–122. doi:10.3354/meps065105

de Boyer Montégut, C., G. Madec, A. S. Fischer, A. Lazar, and D. Iudicone. 2004. Mixed layer depth over the global ocean: An examination of profile data and a profile-based climatology. J. Geophys. Res. Oceans **109**: C12003. doi:10.1029/2004JC002378

Dutkiewicz, S., M. J. Follows, and P. Parekh. 2005. Interactions of the iron and phosphorus cycles: A three-dimensional model study. Global Biogeochem. Cycles **19**: GB1021. doi:10.1029/2004GB002342

Elser, J. J., D. R. Dobberfuhl, N. A. MacKay, and J. H. Schampel. 1996. Organism size, life history, and N:P stoichiometry. BioScience **46**: 674–684. doi:10.2307/1312897

Fennel, K., and E. Boss. 2003. Subsurface maxima of phytoplankton and chlorophyll: Steady-state solutions from a simple model. Limnol. Oceanogr. **48**: 1521–1534. doi:10.4319/lo.2003.48.4.1521

Fiala, M., E. E. Kopczynska, L. Oriol, and M.-C. Machado. 2004. Phytoplankton variability in the Crozet Basin frontal zone (Southwest Indian Ocean) during austral summer. J. Mar. Syst. **50**: 243–261. doi:10.1016/j.jmarsys.2004.01.008

Gall, M. P., P. W. Boyd, J. Hall, K. A. Safi, and H. Chang. 2001. Phytoplankton processes. Part 1: Community structure during the Southern Ocean Iron RElease Experiment (SOIREE). Deep Sea Res. Part II Top. Stud. Oceanogr. **48**: 2551–2570. doi:10.1016/S0967-0645(01)00008-X

Golz, A.-L., A. Burian, and M. Winder. 2015. Stoichiometric regulation in micro- and mesozooplankton. J. Plankton Res. **37**: 293–305. doi:10.1093/plankt/fbu109

Gomi, Y., M. Fukuchi, and A. Taniguchi. 2010. Diatom assemblages at subsurface chlorophyll maximum layer in the eastern Indian sector of the Southern Ocean in summer. J. Plankton Res. **32**: 1039–1050. doi:10.1093/plankt/fbq031

Gordon, H. R., and W. R. McCluney. 1975. Estimation of the depth of sunlight penetration in the sea for remote sensing. Appl. Opt. **14**: 413–416. doi:10.1364/AO.14.000413

Hasle, G. R., and E. E. Syvertsen. 1997. Chapter 2—marine diatoms, p. 5–385. In C. R. Tomas [ed.], Identifying marine phytoplankton. Academic Press.

Henjes, J., P. Assmy, C. Klaas, P. Verity, and V. Smetacek. 2007. Response of microzooplankton (protists and small copepods) to an iron-induced phytoplankton bloom in the Southern Ocean (EisenEx). Deep Sea Res. Part I Oceanogr. Res. Pap. **54**: 363–384. doi:10.1016/j.dsr.2006.12.004

Hillebrand, H., C.-D. Dürselen, D. Kirschtel, U. Pollingher, and T. Zohary. 1999. Biovolume calculation for pelagic and benthic microalgae. J. Phycol. **35**: 403–424. doi:10.1046/j.1529-8817.1999.3520403.x

Ho, T.-Y., A. Quigg, Z. V. Finkel, A. J. Milligan, K. Wyman, P. G. Falkowski, and F. M. M. Morel. 2003. The elemental composition of some marine phytoplankton. J. Phycol. **39**: 1145–1159. doi:10.1111/j.0022-3646.2003.03-090.x

Hoffmann, L. J., I. Peeken, K. Lochte, P. Assmy, and M. Veldhuis. 2006. Different reactions of Southern Ocean phytoplankton size classes to iron fertilization. Limnol. Oceanogr. **51**: 1217–1229. doi:10.4319/lo.2006.51.3.1217

Hoffmann, L. J., I. Peeken, and K. Lochte. 2007. Effects of iron on the elemental stoichiometry during EIFEX and in the diatoms Fragilariopsis kerguelensis and Chaetoceros dichaeta. Biogeosciences **4**: 569–579. doi:10.5194/bg-4-569-2007

Holm-Hansen, O., and C. D. Hewes. 2004. Deep chlorophyll-a maxima (DCMs) in Antarctic waters. I. Relationships between DCMs and the physical, chemical, and optical conditions in the upper water column. Polar Biol. **27**: 699–710. doi:10.1007/s00300-004-0641-1

Holm-Hansen, O., M. Kahru, and C. Hewes. 2005. Deep chlorophyll a maxima (DCMs) in pelagic Antarctic waters. II. Relation to bathymetric features and dissolved iron concentrations. Mar. Ecol. Prog. Ser. **297**: 71–81. doi:10.3354/meps297071

Howard, A. G., A. J. Coxhead, I. A. Potter, and A. P. Watt. 1986. Determination of dissolved aluminium by the micelle-enhanced fluorescence of its lumogallion complex. Analyst **111**: 1379–1382. doi:10.1039/AN9861101379

Hutchins, D. A., and K. W. Bruland. 1998. Iron-limited diatom growth and Si:N uptake ratios in a coastal upwelling regime. Nature **393**: 561–564. doi:10.1038/31203

Jacquet, S. H., P. J. Lam, T. Trull, and F. Dehairs. 2011. Carbon export production in the Subantarctic zone and polar front zone south of Tasmania. Deep Sea Res. Part II Top. Stud. Oceanogr. **58**: 2277–2292. doi:10.1016/j.dsr2.2011.05.035

Johnston, T. M. S., and D. L. Rudnick. 2009. Observations of the Transition Layer. J. Phys. Oceanogr. **39**: 780–797. doi:10.1175/2008JPO3824.1

Khatiwala, S., F. Primeau, and T. Hall. 2009. Reconstruction of the history of anthropogenic CO_2 concentrations in the ocean. Nature **462**: 346–349. doi:10.1038/nature08526

Klausmeier, C. A., E. Litchman, T. Daufresne, and S. A. Levin. 2004. Optimal nitrogen-to-phosphorus stoichiometry of phytoplankton. Nature **429**: 171–174. doi:10.1038/nature02454

Kopczynska, E. E., F. Dehairs, M. Elskens, and S. Wright. 2001. Phytoplankton and microzooplankton variability between the Subtropical and Polar Fronts south of Australia: Thriving under regenerative and new production in late summer. J. Geophys. Res. Oceans **106**: 31597–31609. doi:10.1029/2000JC000278

Kopczyńska, E. E., and M. Fiala. 2003. Surface phytoplankton composition and carbon biomass distribution in the Crozet Basin during austral summer of 1999: Variability across frontal zones. Polar Biol. **27**: 17–28. doi:10.1007/s00300-003-0564-2

Korb, R. E., and M. Whitehouse. 2004. Contrasting primary production regimes around South Georgia, Southern Ocean: Large blooms versus high nutrient, low chlorophyll waters. Deep Sea Res. Part I Oceanogr. Res. Pap. **51**: 721–738. doi:10.1016/j.dsr.2004.02.006

Korb, R. E., M. J. Whitehouse, A. Atkinson, and S. E. Thorpe. 2008. Magnitude and maintenance of the phytoplankton bloom at South Georgia: A naturally iron-replete environment. Mar. Ecol. Prog. Ser. **368**: 75–91. doi:10.3354/meps07525

Korb, R. E., M. J. Whitehouse, M. Gordon, P. Ward, and A. J. Poulton. 2010. Summer microplankton community structure across the Scotia Sea: Implications for biological carbon export. Biogeosciences **7**: 343–356. doi:10.5194/bg-7-343-2010

Kuwata, A., and A. Tsuda. 2005. Selection and viability after ingestion of vegetative cells, resting spores and resting cells of the marine diatom, Chaetoceros pseudocurvisetus, by two copepods. J. Exp. Mar. Biol. Ecol. **322**: 143–151. doi:10.1016/j.jembe.2005.02.013

Lam, P. J., and J. K. B. Bishop. 2007. High biomass, low export regimes in the Southern Ocean. Deep Sea Res. Part II Top. Stud. Oceanogr. **54**: 601–638. doi:10.1016/j.dsr2.2007.01.013

Lam, P. J., S. C. Doney, and J. K. B. Bishop. 2011. The dynamic ocean biological pump: Insights from a global compilation of particulate organic carbon, CaCO3, and opal concentration profiles from the mesopelagic. Global Biogeochem. Cycles **25**: GB3009. doi:10.1029/2010GB003868

Landry, M. R., and A. Calbet. 2004. Microzooplankton production in the oceans. ICES J. Mar. Sci. J. Cons. **61**: 501–507. doi:10.1016/j.icesjms.2004.03.011

Lasbleiz, M., K. Leblanc, S. Blain, J. Ras, V. Cornet-Barthaux, S. Hélias Nunige, and B. Quéguiner. 2014. Pigments, elemental composition (C, N, P, and Si), and stoichiometry of particulate matter in the naturally iron fertilized region of Kerguelen in the Southern Ocean. Biogeosciences **11**: 5931–5955. doi:10.5194/bg-11-5931-2014

Legendre, L., and J. Le Fèvre. 1989. Hydrodynamical singularities as controls of recycled versus export production in oceans, p. 49–63. In W. H. Berger, V. S. Smetacek, G. Wefer [eds.], Productivity of the oceans: Present and past. John Wiley & Sons.

Legendre, P., and L. Legendre. 1998. Numerical ecology, 2nd ed. Elsevier Science.

Legendre, L., and R. B. Rivkin. 2015. Flows of biogenic carbon within marine pelagic food webs: Roles of microbial competition switches. Mar. Ecol. Prog. Ser. **521**: 19–30. doi:10.3354/meps11124

Letelier, R. M., D. M. Karl, M. R. Abbott, and R. R. Bidigare. 2004. Light driven seasonal patterns of chlorophyll and nitrate in the lower euphotic zone of the North Pacific Subtropical Gyre. Limnol. Oceanogr. **49**: 508–519. doi:10.4319/lo.2004.49.2.0508

Maiti, K., M. A. Charette, K. O. Buesseler, and M. Kahru. 2013. An inverse relationship between production and export efficiency in the Southern Ocean. Geophys. Res. Lett. **40**: 1557–1561. doi:10.1002/grl.50219

Malzahn, A. M., F. Hantzsche, K. L. Schoo, M. Boersma, and N. Aberle. 2010. Differential effects of nutrient-limited primary production on primary, secondary or tertiary consumers. Oecologia **162**: 35–48. doi:10.1007/s00442-009-1458-y

Margalef, R. 1958. Temporal succession and spatial heterogeneity in phytoplankton, p. 323–349. In A. A. Buzzati-Traverso [eds.], Perspective in marine biology. University of California.

Margalef, R. 1978. Life-forms of phytoplankton as survival alternatives in an unstable environment. Oceanol. Acta **1**: 493–509.

Martin, J. H. 1990. Glacial-interglacial CO_2 change: The Iron Hypothesis. Paleoceanography **5**: 1–13. doi:10.1029/PA005i001p00001

Martin, J., and others. 2010. Prevalence, structure and properties of subsurface chlorophyll maxima in Canadian

Arctic waters. Mar. Ecol. Prog. Ser. **412**: 69–84. doi:10.3354/meps08666

Martiny, A. C., C. T. A. Pham, F. W. Primeau, J. A. Vrugt, J. K. Moore, S. A. Levin, and M. W. Lomas. 2013. Strong latitudinal patterns in the elemental ratios of marine plankton and organic matter. Nat. Geosci. **6**: 279–283. doi:10.1038/ngeo1757

Menden-Deuer, S., and E. J. Lessard. 2000. Carbon to volume relationships for dinoflagellates, diatoms, and other protist plankton. Limnol. Oceanogr. **45**: 569–579. doi:10.4319/lo.2000.45.3.0569

Mignot, A., H. Claustre, J. Uitz, A. Poteau, F. D'Ortenzio, and X. Xing. 2014. Understanding the seasonal dynamics of phytoplankton biomass and the deep chlorophyll maximum in oligotrophic environments: A Bio-Argo float investigation. Glob. Biogeochem. Cycles **28**: 2013GB004781. doi:10.1002/2013GB004781

Minas, H. J., M. Minas, and T. T. Packard. 1986. Productivity in upwelling areas deduced from hydrographic and chemical fields. Limnol. Oceanogr. **31**: 1182–1206. doi:10.4319/lo.1986.31.6.1182

Moore, C. M., A. E. Hickman, A. J. Poulton, S. Seeyave, and M. I. Lucas. 2007. Iron–light interactions during the CROZet natural iron bloom and EXport experiment (CROZEX): II—Taxonomic responses and elemental stoichiometry. Deep Sea Res. Part II Top. Stud. Oceanogr. **54**: 2066–2084. doi:10.1016/j.dsr2.2007.06.015

Morel, A., and J.-F. Berthon. 1989. Surface pigments, algal biomass profiles, and potential production of the euphotic layer: Relationships reinvestigated in view of remote-sensing applications. Limnol. Oceanogr. **34**: 1545–1562. doi:10.4319/lo.1989.34.8.1545

Mosseri, J., B. Quéguiner, L. Armand, and V. Cornet-Barthaux. 2008. Impact of iron on silicon utilization by diatoms in the Southern Ocean: A case study of Si/N cycle decoupling in a naturally iron-enriched area. Deep Sea Res. Part II Top. Stud. Oceanogr. **55**: 801–819. doi:10.1016/j.dsr2.2007.12.003

Neveux, J., and F. Lantoine. 1993. Spectrofluorometric assay of chlorophylls and phaeopigments using the least squares approximation technique. Deep Sea Res. Part I Oceanogr. Res. Pap. **40**: 1747–1765. doi:10.1016/0967-0637(93)90030-7

Obernosterer, I., U. Christaki, D. Lefèvre, P. Catala, F. Van Wambeke, and P. Lebaron. 2008. Rapid bacterial mineralization of organic carbon produced during a phytoplankton bloom induced by natural iron fertilization in the Southern Ocean. Deep Sea Res. Part II Top. Stud. Oceanogr. **55**: 777–789. doi:10.1016/j.dsr2.2007.12.005

Obernosterer, I., P. Catala, P. Lebaron, and N. J. West. 2011. Distinct bacterial groups contribute to carbon cycling during a naturally iron fertilized phytoplankton bloom in the Southern Ocean. Limnol. Oceanogr. **56**: 2391–2401. doi:10.4319/lo.2011.56.6.2391

Park, Y.-H., E. Charriaud, D. R. Pino, and C. Jeandel. 1998. Seasonal and interannual variability of the mixed layer properties and steric height at station KERFIX, southwest of Kerguelen. J. Mar. Syst. **17**: 571–586. doi:10.1016/S0924-7963(98)00065-7

Park, J., I.-S. Oh, H.-C. Kim, and S. Yoo. 2010. Variability of SeaWiFs chlorophyll-a in the southwest Atlantic sector of the Southern Ocean: Strong topographic effects and weak seasonality. Deep Sea Res. Part I Oceanogr. Res. Pap. **57**: 604–620. doi:10.1016/j.dsr.2010.01.004

Park, Y.-H., J.-H. Lee, I. Durand, and C.-S. Hong. 2014. Validation of Thorpe-scale-derived vertical diffusivities against microstructure measurements in the Kerguelen region. Biogeosciences **11**: 6927–6937. doi:10.5194/bg-11-6927-2014

Parslow, J. S., P. W. Boyd, S. R. Rintoul, and F. B. Griffiths. 2001. A persistent subsurface chlorophyll maximum in the Interpolar Frontal Zone south of Australia: Seasonal progression and implications for phytoplankton-light-nutrient interactions. J. Geophys. Res. Oceans **106**: 31543–31557. doi:10.1029/2000JC000322

Pollard, R. T., H. J. Venables, J. F. Read, and J. T. Allen. 2007. Large-scale circulation around the Crozet Plateau controls an annual phytoplankton bloom in the Crozet Basin. Deep Sea Res. Part II Top. Stud. Oceanogr. **54**: 1915–1929. doi:10.1016/j.dsr2.2007.06.012

Poulton, A. J., C. Mark Moore, S. Seeyave, M. I. Lucas, S. Fielding, and P. Ward. 2007. Phytoplankton community composition around the Crozet Plateau, with emphasis on diatoms and Phaeocystis. Deep Sea Res. Part II Top. Stud. Oceanogr. **54**: 2085–2105. doi:10.1016/j.dsr2.2007.06.005

Price, N. M. 2005. The elemental stoichiometry and composition of an iron-limited diatom. Limnol. Oceanogr. **50**: 1159–1171. doi:10.4319/lo.2005.50.4.1159

Price, N. M., B. A. Ahner, and F. M. M. Morel. 1994. The equatorial Pacific Ocean: Grazer-controlled phytoplankton populations in an iron-limited ecosystem. Limnol. Oceanogr. **39**: 520–534. doi:10.4319/lo.1994.39.3.0520

Primeau, F. W., M. Holzer, and T. DeVries. 2013. Southern Ocean nutrient trapping and the efficiency of the biological pump. J. Geophys. Res. Oceans **118**: 2547–2564. doi:10.1002/jgrc.20181

Pujo-Pay, M., and P. Raimbault. 1994. Improvement of the wet-oxidation procedure for simultaneous determination of particulate organic nitrogen and phosphorus collected on filters. Mar. Ecol. Prog. Ser. **105**: 203–207. doi:10.3354/meps105203

Quéguiner, B. 2013. Iron fertilization and the structure of planktonic communities in high nutrient regions of the Southern Ocean. Deep Sea Res. Part II Top. Stud. Oceanogr. **90**: 43–54. doi:10.1016/j.dsr2.2012.07.024

Quéguiner, B., and M. A. Brzezinski. 2002. Biogenic silica production rates and particulate organic matter distribution in the Atlantic sector of the Southern Ocean during austral spring 1992. Deep Sea Res. Part II Top. Stud. Oceanogr. **49**: 1765–1786. doi:10.1016/S0967-0645(02)00011-5

Quigg, A., and others. 2003. The evolutionary inheritance of elemental stoichiometry in marine phytoplankton. Nature **425**: 291–294. doi:10.1038/nature01953

Ragueneau, O., N. Savoye, Y. Del Amo, J. Cotten, B. Tardiveau, and A. Leynaert. 2005. A new method for the measurement of biogenic silica in suspended matter of coastal waters: Using Si:Al ratios to correct for the mineral interference. Cont. Shelf Res. **25**: 697–710. doi:10.1016/j.csr.2004.09.017

Redfield, A. C. 1958. The biological control of chemical factors in the environment. Am. Sci. **11**: 205–221.

Rembauville, M., S. Blain, L. Armand, B. Quéguiner, and I. Salter. 2015a. Export fluxes in a naturally iron-fertilized area of the Southern Ocean—Part 2: Importance of diatom resting spores and faecal pellets for export. Biogeosciences **12**: 3171–3195. doi:10.5194/bg-12-3171-2015

Rembauville, M., I. Salter, N. Leblond, A. Gueneugues, and S. Blain. 2015b. Export fluxes in a naturally iron-fertilized area of the Southern Ocean—Part 1: Seasonal dynamics of particulate organic carbon export from a moored sediment trap. Biogeosciences **12**: 3153–3170. doi:10.5194/bg-12-3153-2015

Rigual-Hernández, A. S., T. W. Trull, S. G. Bray, A. Cortina, and L. K. Armand. 2015. Latitudinal and temporal distributions of diatom populations in the pelagic waters of the Subantarctic and Polar Frontal zones of the Southern Ocean and their role in the biological pump. Biogeosciences **12**: 5309–5337. doi:10.5194/bg-12-5309-2015

Sabine, C. L., and others. 2004. The oceanic sink for anthropogenic CO_2. Science **305**: 367–371. doi:10.1126/science.1097403

Salter, I., and others. 2007. Estimating carbon, silica and diatom export from a naturally fertilised phytoplankton bloom in the Southern Ocean using PELAGRA: A novel drifting sediment trap. Deep Sea Res. Part II Top. Stud. Oceanogr. **54**: 2233–2259. doi:10.1016/j.dsr2.2007.06.008

Salter, I., A. E. S. Kemp, C. M. Moore, R. S. Lampitt, G. A. Wolff, and J. Holtvoeth. 2012. Diatom resting spore ecology drives enhanced carbon export from a naturally iron-fertilized bloom in the Southern Ocean. Global Biogeochem. Cycles **26**: GB1014. doi:10.1029/2010GB003977

Salter, I., R. Schiebel, P. Ziveri, A. Movellan, R. Lampitt, and G. A. Wolff. 2014. Carbonate counter pump stimulated by natural iron fertilization in the Polar Frontal Zone. Nat. Geosci. **7**: 885–889. doi:10.1038/ngeo2285

Sarmiento, J. L., N. Gruber, M. A. Brzezinski, and J. P. Dunne. 2004. High-latitude controls of thermocline nutrients and low latitude biological productivity. Nature **427**: 56–60. doi:10.1038/nature02127

Sarthou, G., K. R. Timmermans, S. Blain, and P. Tréguer. 2005. Growth physiology and fate of diatoms in the ocean: A review. J. Sea Res. **53**: 25–42. doi:10.1016/j.seares.2004.01.007

Sarthou, G., D. Vincent, U. Christaki, I. Obernosterer, K. R. Timmermans, and C. P. D. Brussaard. 2008. The fate of biogenic iron during a phytoplankton bloom induced by natural fertilisation: Impact of copepod grazing. Deep Sea Res. Part II Top. Stud. Oceanogr. **55**: 734–751. doi:10.1016/j.dsr2.2007.12.033

Shih, L. H., J. R. Koseff, G. N. Ivey, and J. H. Ferziger. 2005. Parameterization of turbulent fluxes and scales using homogeneous sheared stably stratified turbulence simulations. J. Fluid Mech. **525**: 193–214. doi:10.1017/S0022112004002587

Smetacek, V. S. 1985. Role of sinking in diatom life-history cycles: Ecological, evolutionary and geological significance. Mar. Biol. **84**: 239–251. doi:10.1007/BF00392493

Smetacek, V., P. Assmy, and J. Henjes. 2004. The role of grazing in structuring Southern Ocean pelagic ecosystems and biogeochemical cycles. Antarct. Sci. **16**: 541–558. doi:10.1017/S0954102004002317

Sterner, R. W., and J. J. Elser. 2002. Ecological stoichiometry: The biology of elements from molecules to the biosphere. Princeton University Press.

Strzepek, R. F., K. A. Hunter, R. D. Frew, P. J. Harrison, and P. W. Boyd. 2012. Iron-light interactions differ in Southern Ocean phytoplankton. Limnol. Oceanogr. **57**: 1182–1200. doi:10.4319/lo.2012.57.4.1182

Tagliabue, A., J.-B. Sallée, A. R. Bowie, M. Lévy, S. Swart, and P. W. Boyd. 2014. Surface-water iron supplies in the Southern Ocean sustained by deep winter mixing. Nat. Geosci. **7**: 314–320. doi:10.1038/ngeo2101

Takeda, S. 1998. Influence of iron availability on nutrient consumption ratio of diatoms in oceanic waters. Nature **393**: 774–777. doi:10.1038/31674

Timmermans, K. R., W. Stolte, and H. J. W. de Baar. 1994. Iron-mediated effects on nitrate reductase in marine phytoplankton. Mar. Biol. **121**: 389–396. doi:10.1007/BF00346749

Toseland, A., and others. 2013. The impact of temperature on marine phytoplankton resource allocation and metabolism. Nat. Clim. Chang. **3**: 979–984. doi:10.1038/nclimate1989

Uitz, J., H. Claustre, F. B. Griffiths, J. Ras, N. Garcia, and V. Sandroni. 2009. A phytoplankton class-specific primary production model applied to the Kerguelen Islands region (Southern Ocean). Deep Sea Res. Part I Oceanogr. Res. Pap. **56**: 541–560. doi:10.1016/j.dsr.2008.11.006

Van Mooy, B. A. S., and others. 2009. Phytoplankton in the ocean use non-phosphorus lipids in response to phosphorus scarcity. Nature **458**: 69–72. doi:10.1038/nature07659

Venrick, E. L., J. A. McGowan, and A. W. Mantyla. 1973. Deep maxima of photosynthetic chlorophyll in Pacific Ocean. Fish. Bull. **71**: 41–52.

Weber, T. S., and C. Deutsch. 2010. Ocean nutrient ratios governed by plankton biogeography. Nature **467**: 550–554. doi:10.1038/nature09403

Weston, K., L. Fernand, D. K. Mills, R. Delahunty, and J. Brown. 2005. Primary production in the deep chlorophyll maximum of the central North Sea. J. Plankton Res. **27**: 909–922. doi:10.1093/plankt/fbi064

Whitehouse, M. J., J. Priddle, and M. A. Brandon. 2000. Chlorophyll/nutrient characteristics in the water masses to the north of South Georgia, Southern Ocean. Polar Biol. **23**: 373–382. doi:10.1007/s003000050458

Acknowledgments

We thank the captain Bernard Lassiette and crew of the R/V Marion Dufresne for their support aboard as well as the chief scientist Yves Cherel. We thank Claire Lo Monaco and Céline Ridame for the access to the CTD and chlorophyll *a* data and Isabelle Durand for the help in the Thorpe displacement calculation. We thank the three anonymous reviewers for their constructive comments, which helped us to improve the manuscript. This work was supported by grants from the French research program of INSU-CNRS LEFE-CYBER (EXPLAIN, Ian Salter) and the French ANR (KEOPS2, ANR-10-BLAN-0614, Stéphane Blain). The OISO program is supported by the French institutes INSU and IPEV, the French program SOERE/Great-gases, and the European program FP7/Carbochange.

Submitted 15 June 2015
Revised 22 January 2016
Accepted 18 February 2016

Associate editor: Anya Waite